ORGANOMETALLICS
Article
Cite This: Organometallics XXXX, XXX, XXX−XXX
pubs.acs.org/Organometallics

Coordination Behavior of *N,N′,N″*-Trisubstituted Guanidine Ligands in Their Ru−Arene Complexes: Synthetic, DNA/Protein Binding, and Cytotoxic Studies

Kumaramangalam Jeyalakshmi,[†,‡] Jebiti Haribabu,[†] Chandrasekar Balachandran,[§] Srividya Swaminathan,[†] Nattamai S. P. Bhuvanesh,[∥] and Ramasamy Karvembu*[,†]

[†]Department of Chemistry, National Institute of Technology, Tiruchirappalli 620015, India
[‡]Department of Science and Humanities, M. Kumarasamy College of Engineering, Karur 639113, India
[§]Department of Hematology, Fujita Health University, 1-98, Dengakugakubo, Kutsukake-cho, Toyoake, Aichi 470-1192, Japan
[∥]Department of Chemistry, Texas A&M University, College Station, Texas 77842, United States

Supporting Information

ABSTRACT: Ruthenium complexes are fascinating for exploration as anticancer drugs after the entry of KP1019 and NAMI-A in phase II clinical trials for the treatment of metastatic tumors. The reaction of guanidine ligands with $[RuCl(\mu\text{-}Cl)(\eta^6\text{-}p\text{-cymene})]_2$ yielded monometallic Ru(II) complexes with N,N-type (**1**) and O,N-type (**2** and **3**) ligands, whereas both monometallic (O,N) (**7**) and bimetallic Ru(II) (**4**−**6**) complexes were obtained when $[RuCl(\mu\text{-}Cl)(\eta^6\text{-benzene})]_2$ was used as a precursor. The complexes were characterized using analytical, spectroscopic (UV−vis, FT-IR, NMR, and mass), and single-crystal X-ray crystallography techniques. The stability of the complexes was tested by UV−visible spectroscopy. The complexes were investigated for their interaction with calf thymus (CT) DNA and bovine serum albumin using various spectroscopic techniques. Spectroscopic and viscosity experiments revealed that the intrinsic DNA binding affinity of the Ru−*p*-cymene complexes was greater than that of the analogous Ru−benzene complexes due to the increased hydrophobicity of the *p*-cymene ring. The in vitro cytotoxicity of the complexes against HepG2, A549, and Vero cells was evaluated using MTT assay. The results revealed that the complexes with O,N bidentate-type ligands, **2** and **3**, showed good activity against HepG2 cell lines with an IC_{50} value of 15.41 and 17.74 μM, respectively. The results were compared with cisplatin, and it was inferred that complexes **2** and **3** showed better activity than cisplatin. The apoptosis mode of cell death was confirmed by staining and flow cytometry methods.

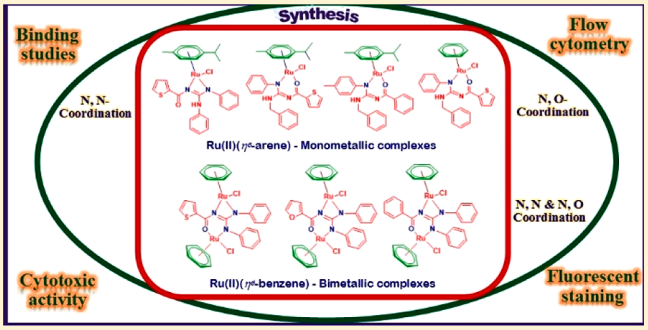

INTRODUCTION

Metallodrugs have become important compounds in cancer therapy; in particular, platinum complexes are used worldwide against many tumor types.[1] Though cisplatin is used as an anticancer drug, its importance has been thwarted by two main disadvantages: it is inefficient against platinum-resistant tumors and has severe side effects such as neuro-, hepto-, and nephrotoxicity.[2] Therefore, the quest for alternative drugs to the well-known cisplatin and its derivatives is highly needed. In this context, ruthenium complexes are noted as anticancer agents due to similar ligand exchange kinetics with that of the platinum(II) complexes.[3,4] The Ru(III) complexes NAMI-A and KP1019 have shown the most promising results in preclinical and clinical studies.[5−7] Most recently, organometallic ruthenium(II) complexes especially half-sandwich Ru(II)−arene complexes are fascinating as therapeutics because their biological activity can be tuned by varying the ligands. The good examples for this type of complexes are RAPTA family[8] containing 1,3,5-triaza-7-phosphatricyclo[3.3.1.1]decane ligand and Ru−arene complexes containing bidentate ethylenediamine, which are at an advanced preclinical trial (Figure 1).[9]

Complexes of the type $[(\eta^6\text{-arene})Ru(X)(YZ)]$ (where YZ is a bidentate chelating ligand and X is a good leaving group) exhibit both in vitro and in vivo anticancer activity; some cases are even comparable with cisplatin.[10] The aqueous reactivity of $[(\eta^6\text{-arene})Ru(X)(YZ)]$ complexes is highly dependent on the nature of X, YZ, and the arene. $[(\eta^6\text{-Arene})Ru(ethylenediamine)Cl]^+$ complexes exhibit anticancer activity both in vitro and in vivo against cisplatin-resistant cancer cells.[11a] It is expected that Cl^- always serves as a better leaving group where hydrolysis takes place consequently. Therefore, the aqueous reactivity is dependent on the choice of ligand

Received: September 26, 2018

DOI: 10.1021/acs.organomet.8b00702
Organometallics XXXX, XXX, XXX−XXX

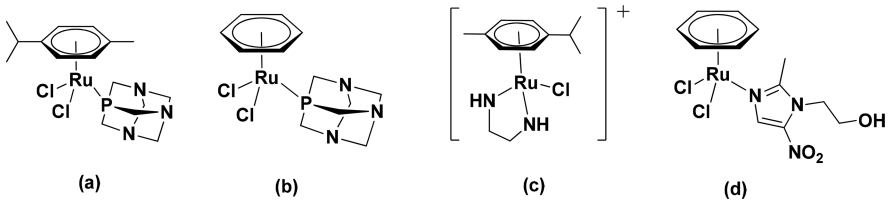

Figure 1. Ru−arene anticancer complexes (a) RAPTA-C, (b) RAPTA-B, (c) [(η^6-arene)Ru(ethylenediamine)Cl]$^+$, and (d) [(η^6-benzene)Ru(metronidazole)Cl_2].

Scheme 1. Structure of the Ligands

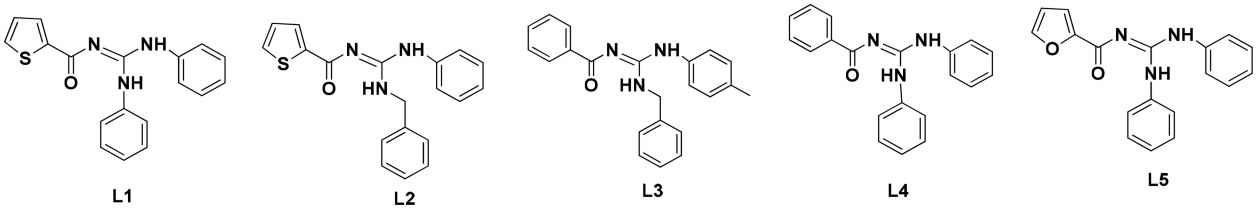

Scheme 2. Synthesis of the Ru(II)(η^6-*p*-cymene) Complexes

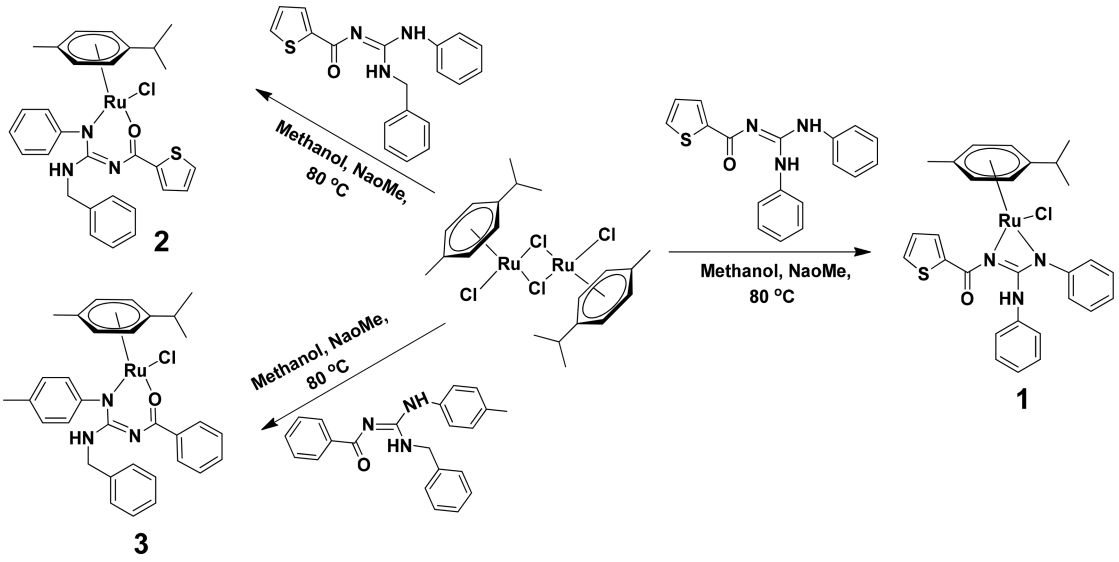

system. In the complexes containing diimine ligands, the higher stability of the Ru−Cl bond was related to the electron-withdrawing property of α-diimine ligand.[11b]

Guanidine is an important ingredient in both organic and inorganic chemistry. Guanidine functionalities are found in a variety of natural compounds, either in a cyclic form or as terminal groups of pendant substituents. The guanidine moiety is a part of the arginine molecule in the single protonated form, and it is responsible for the majority of arginine's noncovalent interactions.[12] Some of the naturally occurring guanidines were screened for their nuclease activity and exhibited cytotoxic properties. Guanidine is noted as a sterically and electronically flexible ligand because of the Y-shaped CN_3 unit present in it. Guanidines have a broad spectrum of biological activities, such as antitumor,[13−15] antimalarial, anti-inflammatory, urease inhibition,[16] etc. This is further enhanced by coordination with metal. The possible coordination modes of guanidines are (i) neutral guanidines,[17,18] (ii) monoanionic guanidinates [guanidinates (−1)],[19,20] and (iii) dianionic guanidinates [guanidinates (−2)].[21,22]

The different coordination possibilities of the ligand when interacting with transition metals will be helpful in tuning up the pharmacological properties. The difference in the donor atoms (N,N and N,O) will have an influence on the rate of hydrolysis, which is crucial in the cytotoxicity of the metallodrugs, particularly of the type [RuCl(arene)L].[23] Fascinated by the biological importance of ruthenium−arene complexes and guanidines, herein, we report the synthesis of Ru−arene complexes containing trisubstituted guanidine ligands. Moreover, the biological applications of complexes of guanidines have not been explored much. This motivates us to study the biological applications of guanidine-based Ru−arene complexes. The novel complexes were characterized by various spectroscopic techniques and investigated for their biological applications. To our knowledge, this is the first report on ruthenium bimetallic complexes containing trisubstituted guanidine ligands.

RESULTS AND DISCUSSION

Synthesis of the Ligands and Complexes. The ligands (**L1**−**L4**) were synthesized by using the procedure reported

DOI: 10.1021/acs.organomet.8b00702
Organometallics XXXX, XXX, XXX−XXX

Scheme 3. Synthesis of the Ru(II)(η^6-benzene) Complexes

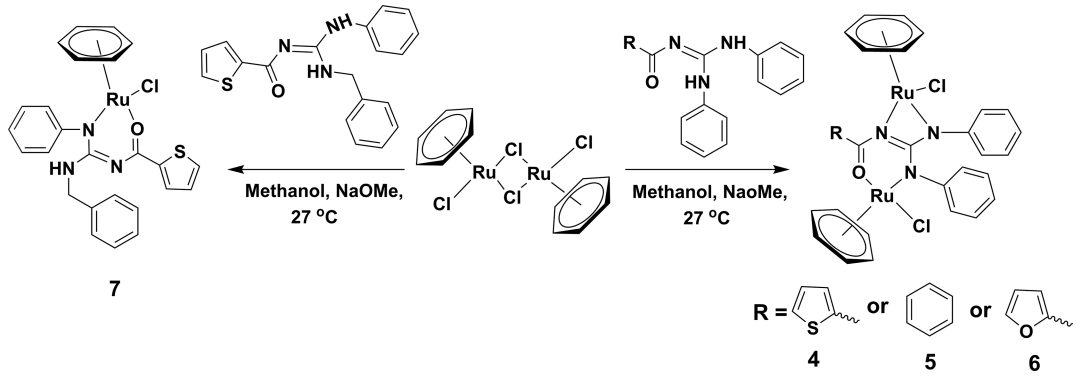

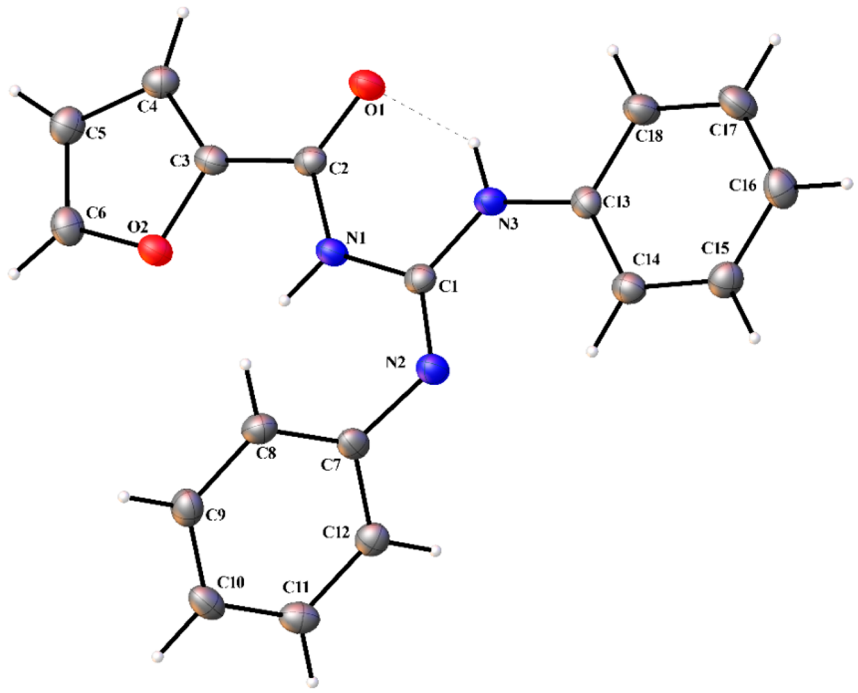

Figure 2. Thermal ellipsoid (50%) plot of **L5**.

earlier.[24−26] **L5** was prepared from *N*-furoyl-*N*′-phenylthiourea by the guanylation method. The ligands used in this work are shown in Scheme 1.

Interaction of ligands **L1**−**L3** with [RuCl(μ-Cl)(η^6-*p*-cymene)]$_2$ yielded monometallic ruthenium(η^6-*p*-cymene) complexes **1**−**3**, where the donor atoms of guanidines were different (N,N/N,O) when the substitution was changed (Scheme 2). The reaction of ligands **L1**, **L2**, **L4**, and **L5** with [RuCl(μ-Cl)(η^6-benzene)]$_2$ ended up with the formation of monometallic **7** and bimetallic complexes **4**−**6** (Scheme 3).

Spectroscopy. The synthesized Ru−arene complexes were characterized by UV−vis, Fourier transform infrared (FT-IR), NMR, and mass spectroscopic techniques. The band appeared in the UV−vis spectra of the complexes in the 422−454 nm region indicated d → d transition in the complexes. The band at 319−334 nm in the spectra of complexes **3**, **5**, and **6** was due to the metal to ligand charge transfer transition.

In the FT-IR spectra of the ligands, two bands (strong and weak) were observed for the N−H group in the range of 3394−3145 cm^{-1}. The weak band is due to the hydrogen bonded N−H. The C═O and C═N stretching frequencies were observed around 1611−1590 and 1571−1558 cm^{-1}, respectively. On complexation (complex **1**), there was a disappearance of one N−H band and a decrease in the imine stretching frequency, indicating that the coordination occurred through imine and N−H nitrogen atoms. In the FT-IR spectra of complexes **2**, **3**, and **7**, there was a disappearance of one N−H band and shift in the carbonyl stretching frequency to a lower value, which clearly indicated the O,N coordination of the ligands. There was a disappearance of two N−H bands and shift in C═O stretching frequency in the FT-IR spectra of complexes **4**, **5**, and **6**, which indicated the coordination of carbonyl oxygen, imine nitrogen, and two N−H nitrogen atoms after deprotonation, forming bimetallic Ru−arene complexes. Interestingly, this is a rare coordination mode of guanidine.

^{1}H and ^{13}C NMR spectral data for **L5** and complexes **1**−**7** are summarized in the Experimental Section, and spectra are depicted in the Supporting Information (Figures S1−S16). In the spectra of the ligands, the N−H (attached to the aromatic ring) peak appeared at 12.07−10.06 ppm and the signal due to N−H (attached to the benzyl group) appeared at 5.25 ppm

DOI: 10.1021/acs.organomet.8b00702
Organometallics XXXX, XXX, XXX−XXX

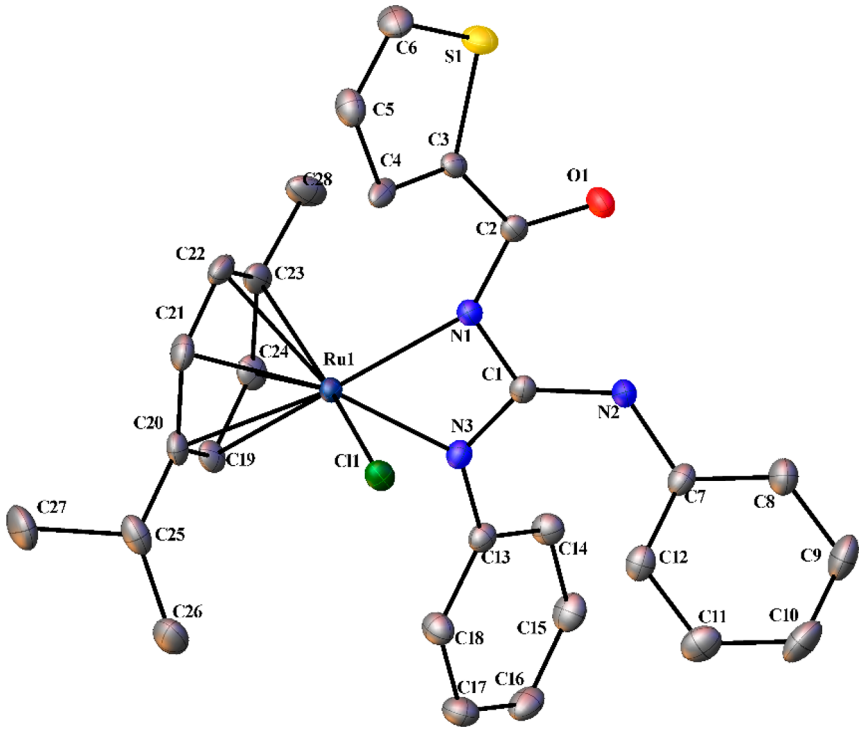

Figure 3. Thermal ellipsoid (50%) plot of **1**. Hydrogen atoms are not shown for clarity.

(**L2** and **L3**). Signals due to aromatic protons of the ligands appeared in the region 8.25−6.45 ppm.[24−26] In the spectra of complexes **1**−**3**, the peak due to N−H proton (12.07−10.30 ppm) disappeared, supporting the coordination of N−H nitrogen after deprotonation. The new signals appeared around 1.23−1.12, 2.63−2.34, and 5.09−3.89 ppm in the spectra of the complexes indicated the presence of the *p*-cymene moiety.[27] In the ^{1}H NMR spectra of complexes **5**, **6**, and **7**, an intense signal at 5.98 ppm confirmed the presence of a benzene moiety in the complexes. In the spectrum of complex **4**, a resonance due to benzene ring protons appeared at 5.11 and 4.95 ppm. There was a disappearance of both the N−H peaks in the spectra of complexes **4**−**6**, which provided evidence for the formation of bimetallic complexes, whereas in complex **7**, there was a disappearance of only one N−H peak and another N−H proton was observed at 5.23 ppm. Chemical shift values of all the other aromatic and aliphatic protons were in the expected range. In the ^{13}C NMR spectra of the complexes, the signals at 176.6−164.2 and 159.5−156.1 ppm were attributed to carbonyl and imine carbons, respectively. The presence of *p*-cymene carbons was confirmed by the signals at 101.5−99.9, 98.5−97.9, 80.8−79.1, 83.7−81.3, 31.2−30.9, 22.6−21.9, and 19−18.3 ppm (complexes **1**−**3**). The signals due to benzene carbons appeared at 88.1−82.3 ppm (complexes **4**−**7**).

Crystal Structures of the Ligand and Complexes. Single crystals suitable for X-ray diffraction analysis were obtained for ligand **L5** and complexes **1**−**7**, and the structures are shown in Figures 2−9. Crystal data and selected interatomic bond lengths and angles are summarized in Tables 1−4. In complexes **1**−**3** and **7**, Ru adopted a pseudo-octahedral piano stool geometry, the arene [**1**−**3** (η^6-*p*-cymene) and **7** (η^6-benzene)] rings displayed the common π-bonded η^6-coordination mode, and the guanidine ligands assumed a bidentate chelate coordination mode (κ^2-N,N or κ^2-O,N). The remaining coordination site was occupied by a chloride ion. Complexes **4**−**6** displayed the same pseudo-octahedral geometry around both the Ru centers. Guanidine acted as a bridging ligand through N,N and O,N donor atoms. The Ru bonded to an arene (η^6-benzene) ring and a chloride ion in addition to bridged guanidine. The Ru−centroid distance in the complexes fell in a narrow range (1.654−1.666 Å) and was similar to that of alike complexes.[28] The Ru−C distances were in the range of 2.129−2.214 Å. The Ru−Cl bond length lay in the range of 2.3916−2.4218 Å,[29] which

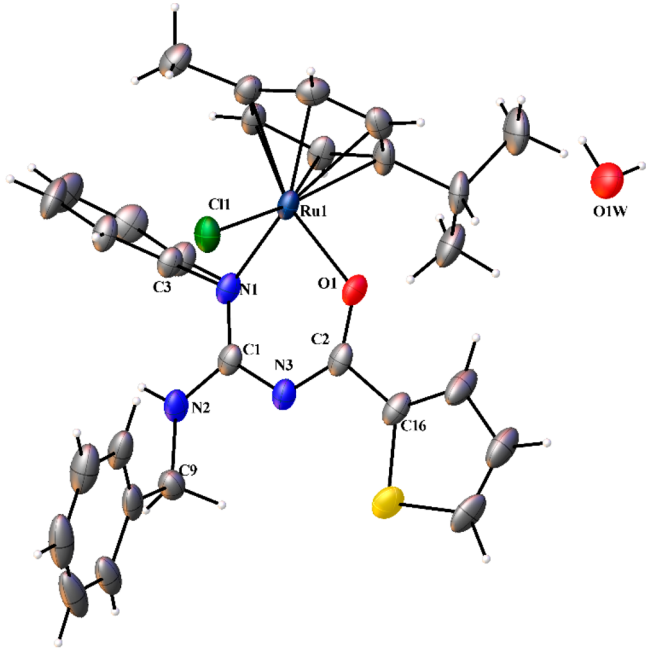

Figure 4. Thermal ellipsoid (50%) plot of **2**. Only selected atoms are labeled for clarity.

DOI: 10.1021/acs.organomet.8b00702
Organometallics XXXX, XXX, XXX−XXX

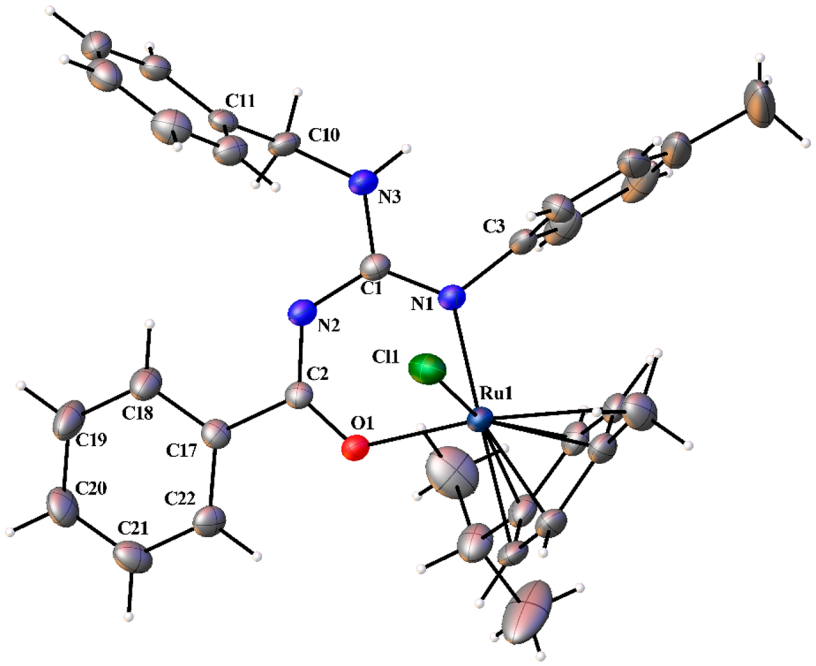

Figure 5. Thermal ellipsoid (50%) plot of **3**. Only selected atoms are labeled for clarity.

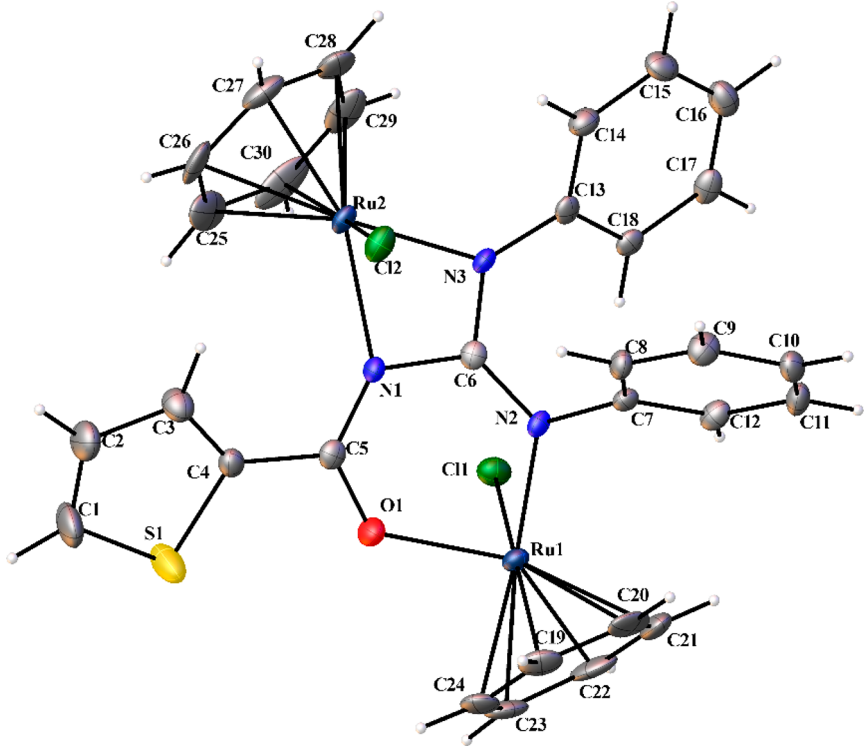

Figure 6. Thermal ellipsoid (50%) plot of **4**.

was longer than the Ru−N (2.068−2.225 Å) and Ru−O (2.056−2.1017 Å) bond lengths. N−Ru−Cl and O−Ru−Cl bond angles were in the range of 83.30−86.67 Å, and the O−Ru−N bond angle was in the range of 84.17−86.01 Å (complexes **2**−**7**). The four-membered chelate ring in complexes **1**, **4**, **5**, and **6** made the N−Ru−N bond angle smaller (60.1−61.83 Å).

Solubility of the Complexes. The solubility measurements revealed that the complexes were less soluble in water and the solubility values were compared with the known anticancer agents (Table S1).

Stability of the Complexes. The stability of complexes plays a crucial role in the development of drugs. The stability of the complexes in a 1% DMSO/water mixture was monitored using UV−visible spectroscopy over a period of 24 h. The complexes exhibited the characteristic bands in their UV−visible spectra (Figure S17). There was no significant change in the spectra of complexes **1**, **2**, **3**, and **7**. Complexes **4**, **5**, and **6**

DOI: 10.1021/acs.organomet.8b00702
Organometallics XXXX, XXX, XXX−XXX

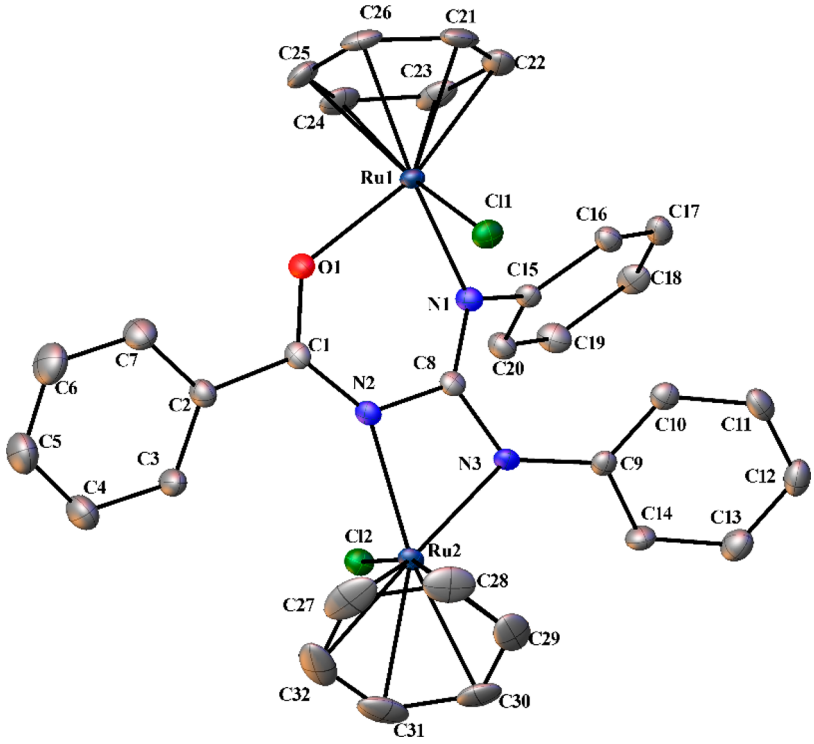

Figure 7. Thermal ellipsoid (50%) plot of **5**. Hydrogen atoms are not shown for clarity.

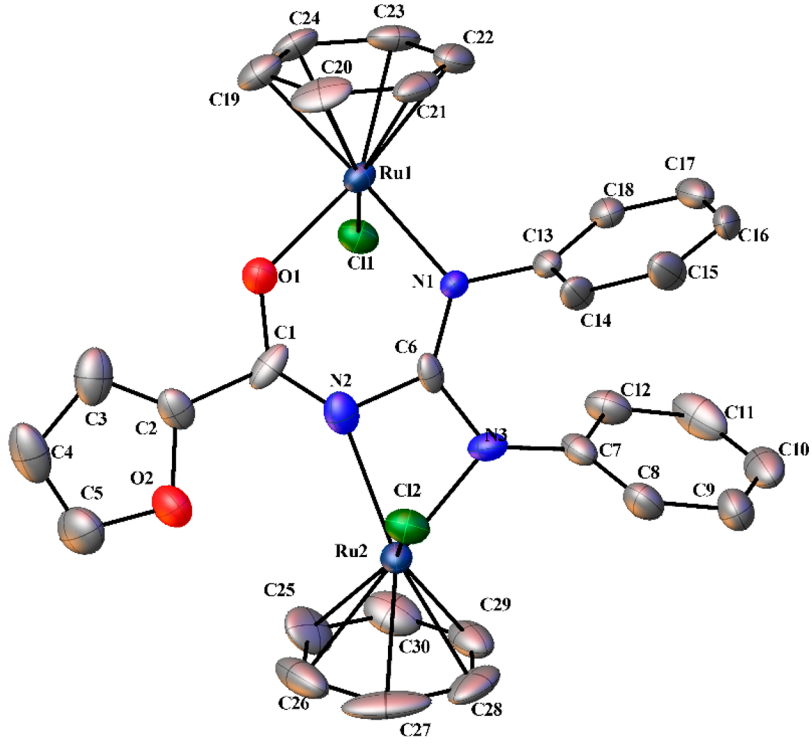

Figure 8. Thermal ellipsoid (50%) plot of **6**. Hydrogen atoms are not shown for clarity.

exhibited shifts in their characteristic band(s). The stable complexes **2**, **3**, and **7** were evaluated for their stability in a 1% DMSO/PBS buffer mixture (Figure S18). There is no shift in the absorption bands of the tested complexes, which clearly indicated the stability of the complexes in the biological medium.[30]

DNA Interaction Studies. DNA binding of the synthesized complexes was evaluated by UV−visible, ethidium bromide displacement, and viscosity studies. The studies revealed that all of the complexes effectively bound with CT DNA. The details are provided in the Supporting Information.

Protein Binding Studies. The molecular targeting and mechanism of action of anticancer drugs are not always

DOI: 10.1021/acs.organomet.8b00702
Organometallics XXXX, XXX, XXX−XXX

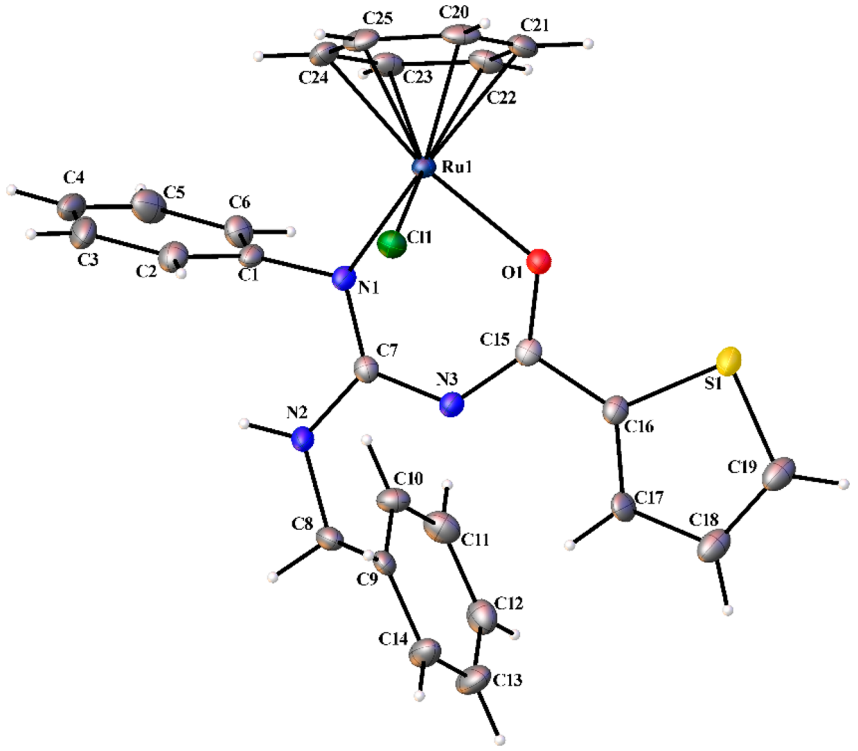

Figure 9. Thermal ellipsoid (50%) plot of **7**.

unambiguous. The cytotoxic complex [(η^6-*p*-cymene)Ru(ethylenediamine)Cl]PF_6 interacted with DNA, whereas the relatively noncytotoxic antimetastasis compound [(η^6-*p*-cymene)Ru(1,3,5-triaza-7-phosphaadamantane)Cl_2] preferentially formed adducts with the histone proteins.[31] Therefore, protein binding studies are also significant for predicting the mechanism of action of anticancer drugs. The binding ability of the complexes with bovine serum albumin (BSA) was evaluated by absorption and fluorescence spectral studies.

Absorption Spectral Studies. The electronic absorption studies are used to explore the type of quenching. The static quenching leads to the perturbation of the fluorophore and results in the absorption spectral changes,[32−36] whereas in dynamic quenching, appreciable change in absorption spectra of the fluorophore is not expected. The absorption spectra of BSA in the absence and presence of the complexes are depicted in Figure S25. For BSA, there were two absorption bands; the one at 213 nm reflected the framework conformation, and the band at 280 nm corresponded to the aromatic amino acids (Trp, Tyr, and Phe) of the protein. Hyperchromism in the absorption band at 280 nm was observed on addition of complexes **1**−**7** to BSA, which clearly indicated the static type of quenching.

Fluorescence Spectral Studies. The fluorescence property of BSA is mainly due to the presence of tryptophan and tyrosine residues. Alteration in the emission spectrum arises primarily from the tryptophan residue because of protein conformational changes, subunit association, substrate binding, or denaturation.[32] The fluorescence titration of complexes **1**−**7** (0−20 μM) with BSA resulted in a decrease in the fluorescence intensity [62.9% (**1**); 63.2% (**2**); 76.8% (**3**); 72.3% (**4**); 72.7% (**5**); 59.2% (**6**); 52.5% (**7**)] with appreciable blue shift (2−4 nm) at 345 nm (excitation wavelength = 280 nm) (Figures 10 and S26). The ability of the complexes to quench the emission intensity was calculated quantitatively using Stern−Volmer equation $F^0/F = 1 + K_q[Q]$, where F^0 and F are fluorescence intensities in the absence and presence of a quencher, respectively, K_q is a linear Stern−Volmer quenching constant, and $[Q]$ is the quencher concentration. The slope of linear plot of F^0/F versus $[Q]$ yielded K_q (Figure 11). Further, the equilibrium binding constant was evaluated using the Scatchard equation, $\log[(F^0 - F)/F] = \log K_b + n \log[Q]$, where K_b is the binding constant and n is the number of the binding site. The K_b values were derived from the graph between $\log[(F^0 - F)/F]$ and $\log[Q]$ (Figure 12). The values of K_b and K_q revealed the enhanced binding ability of complex **3** compared to the other complexes under investigation (Table 5). The calculated values of n (0.8−1) suggested the existence of a single binding site in BSA for all complexes.[37] DNA/protein binding ability of the complexes was comparable with that of the known Ru−arene complexes.[38−42]

Conformational Investigation. To understand the structural changes occurred in BSA on titration with complexes **1**−**7**, synchronous fluorescence studies were carried out.[43] When the concentration of the compounds was increased, the intensity of emission corresponding to tyrosine (304 nm, $\Delta\lambda$ = 15 nm) was found to decrease in the magnitude of 48.5, 52.0, 66.4, 60.8, 58.6, 43.5, and 42.6%, respectively, for complexes **1**−**7** with 2 nm blue shift in the emission wavelength (Figures 13 and S26). The tryptophan fluorescence emission (340 nm, $\Delta\lambda$ = 60 nm) showed a significant decrease in its intensity [62.5 (**1**), 63.8 (**2**), 78.0 (**3**), 70.3 (**4**), 74.8 (**5**), 58.1 (**6**), and 53.1 (**7**)%] without any change in the position of the band (Figures 14 and S27). These results indicated that, although the compounds affected the microenvironments of both tyrosine and tryptophan during the binding process, the effect was more pronounced toward tryptophan.

In Vitro Cytotoxic Activity. The in vitro cytotoxic activity of the Ru−arene complexes (**1**−**7**) was screened against human liver (HepG2), lung carcinoma (A549), and Vero

DOI: 10.1021/acs.organomet.8b00702
Organometallics XXXX, XXX, XXX−XXX

Table 1. Crystal Data and Structure Refinement for Ligand L5 and Complexes 1−3

	L5	1	2	3
empirical formula	$C_{18}H_{15}N_3O_2$	$C_{28}H_{28}ClN_3ORuS$	$C_{29}H_{30\cdot60}ClN_3O_{1\cdot30}RuS$	$C_{32}H_{34}ClN_3ORu$
formula weight	305.33	591.11	610.54	613.14
temperature (K)	110.15	110.15	110.15	110.15
wavelength (Å)	0.71073	0.71073	1.54178	0.71073
crystal system	monoclinic	monoclinic	monoclinic	monoclinic
space group	$P121/c1$	$P121/c1$	$P121/c1$	$P121/c1$
unit cell dimensions				
a (Å)	5.8612(9)	9.3991(18)	10.3394(4)	10.2845(17)
b (Å)	21.505(3)	14.047(3)	27.3435(11)	26.776(4)
c (Å)	12.042(2)	19.692(4)	9.7085(4)	10.3907(17)
α (deg)	90	90	90	90
β (deg)	93.001(2)	90.440(2)	95.913(2)	96.220(2)
γ (deg)	90	90	90	90
volume (Å^3)	1515.7(4)	2599.9(9)	2730.14(19)	2844.5(8)
Z	4	4	4	4
density (calculated) (mg/m^3)	1.338	1.510	1.485	1.432
absorption coefficient (mm^{-1})	0.090	0.812	6.483	0.675
$F(000)$	640	1208	1252	1264
crystal size (mm^3)	0.34 × 0.2 × 0.18	0.25 × 0.2 × 0.18	0.13 × 0.06 × 0.04	0.54 × 0.47 × 0.19
θ range for data collection (deg)	1.894 to 27.531	1.781 to 27.508	4.857 to 59.979	1.521 to 27.407
index ranges	$-7 \le h \le 7$, $-27 \le k \le 26$, $-15 \le l \le 15$	$-12 \le h \le 12$, $-18 \le k \le 18$, $-24 \le l \le 25$	$-11 \le h \le 11$, $-30 \le k \le 30$, $-10 \le l \le 10$	$-13 \le h \le 13$, $-34 \le k \le 34$, $-13 \le l \le 13$
reflections collected	14845	27077	62334	50886
independent reflections [R(int)]	3483 [R(int) = 0.0253]	5937 [R(int) = 0.0259]	4030 [R(int) = 0.0580]	6448 [R(int) = 0.0312]
completeness to θ = 25.242/25.242/60.0/25.242°	99.9	99.8	99.4	100.0
absorption correction	semiempirical from equivalents	semiempirical from equivalents	semiempirical from equivalents	semiempirical from equivalents
max and min transmission	0.7456 and 0.6949	0.7456 and 0.6793	0.7519 and 0.4168	0.7456 and 0.6320
refinement method	full-matrix least-squares on F^2	full-matrix least-squares on F^2	full-matrix least-squares on F^2	full-matrix least-squares on F^2
data/restraints/parameters	3483/0/208	5937/21/319	4030/267/399	6448/0/347
goodness-of-fit on F^2	1.030	1.070	1.143	1.250
final R indices [$I > 2\sigma(I)$]	$R1$ = 0.0383, $wR2$ = 0.0892	R1 = 0.0273, wR2 = 0.0595	R1 = 0.0261, wR2 = 0.0663	R1 = 0.0417, wR2 = 0.0917
R indices (all data)	$R1$ = 0.0468, $wR2$ = 0.0941	R1 = 0.0324, wR2 = 0.0618	R1 = 0.0284, wR2 = 0.0670	R1 = 0.0486, wR2 = 0.0954
largest diff. peak and hole (e·Å^{-3})	0.244 and −0.266	0.532 and −0.499	0.407 and −0.607	0.946 and −0.754

(kidney cells of an African green monkey) cell lines, and the results are provided in Tables 6 and S2−S5 and Figures 15, 16, and S28 and S29. All of the complexes were tested from their low concentration (3.9 μg/mL) to higher concentration (250 μg/mL). In vitro cytotoxic activity investigation revealed that complexes **2** and **3** exhibited high activity against HepG2 cancer cell line at lower concentration of 15.6 μg/mL, with IC_{50} values of 15.41 and 17.74 μM, respectively. Complex **2** was even better than cisplatin in its activity. Complex **7** possessed moderate activity with an IC_{50} value of 59.01 μM. Among all the complexes, complex **2** showed better activity with an IC_{50} value of 58.1 μM against A549 cancer cell line, whereas the other complexes showed half inhibition above 100 μM. All the complexes were less toxic against normal Vero cell line. The results revealed that the cytotoxic activity of the Ru(II)−arene complexes could be correlated with the donor atoms as (N,O) > (N,N).[44] The results were also in good agreement with the DNA binding efficacy as the (N,O)-type complexes showed a binding ability better than that of the (N,N)-type complexes. It is also important to note that the stable complexes (**2**, **3**, and **7**) exhibited appreciable activity against the cancer cell lines. Unfortunately, the bimetallic complexes did not show marked inhibition.

Our group has reported the cytotoxic activity of Ru(η^6-arene) complexes against A549 and HepG2 cell lines. Mono- and binuclear Ru(η^6-*p*-cymene) complexes containing indole thiosemicarbazone ligands showed appreciable activity against HepG2 and A549 cell lines.[40] Ru(η^6-arene) complexes containing aroylthiourea ligands showed moderate activity against the same cell lines.[41,42] The present complexes, notably **2**, **3** and **7**, showed activity greater than that of the previously reported Ru−arene complexes against HepG2 and A549 cell lines.[45−47] The activity of complexes **2** and **3** was also comparable with that of the reported ruthenium−arene complexes[48−51] against HepG2 and A549 cell lines. It is evident from the comparison that our complexes showed comparable activity with the previously reported ruthenium−arene complexes (Figure 17).

Cell Apoptosis Analysis by Flow Cytometry and Fluorescent Staining Methods. Apoptosis, or programmed cell death, has been used to describe a form of cell death in an active and inherently controlled manner that eliminates no longer wanted cells.[52] Cell and nuclear shrinkage, chromatin condensation, formation of apoptotic bodies, and phagocytosis by neighboring cells characterize the main morphological changes of the apoptosis process.[53] Cleavage of chromosomal DNA into oligonucleosomal size fragments is a biochemical

DOI: 10.1021/acs.organomet.8b00702
Organometallics XXXX, XXX, XXX−XXX

Table 2. Crystal Data and Structure Refinement for Complexes 4−7

	4	5	6	7
empirical formula	$C_{30}H_{25}Cl_2N_3ORu_2S$	$C_{32}H_{27}Cl_2N_3ORu_2$	$C_{30}H_{25}Cl_2N_3O_2Ru_2$	$C_{25}H_{22}ClN_3ORuS$
formula weight	748.63	742.60	732.57	549.03
temperature (K)	110.15	110.15	110.15	110.15
wavelength (Å)	0.71073	0.71073	1.54178	0.71073
crystal system	monoclinic	monoclinic	triclinic	triclinic
space group	$P121/c1$	$P121/c1$	$P\bar{1}$	$P\bar{1}$
unit cell dimensions				
a (Å)	10.072(2)	10.2152(15)	9.5165(4)	8.8195(15)
b (Å)	21.642(5)	21.795(3)	10.5078(4)	10.3836(18)
c (Å)	12.766(3)	12.7780(19)	13.7238(5)	12.827(2)
α (deg)	90	90	86.107(2)	83.215(2)
β (deg)	91.367(2)	90.860(2)	78.282(3)	72.928(2)
γ (deg)	90	90	83.087(3)	83.662(2)
volume (Å^3)	2781.7(10)	2844.5(7)	1332.64(9)	1111.5(3)
Z	4	4	2	2
density (calculated) (mg/m^3)	1.788	1.734	1.826	1.640
absorption coefficient (mm^{-1})	1.383	1.281	11.304	0.943
$F(000)$	1488	1480	728	556
crystal size (mm^3)	0.42 × 0.04 × 0.04	0.25 × 0.21 × 0.17	0.14 × 0.06 × 0.05	0.54 × 0.37 × 0.13
θ range for data collection (deg)	1.853 to 27.582	1.848 to 27.602	3.292 to 60.622	1.981 to 27.490
index ranges	$-13 \le h \le 13$, $-28 \le k \le 28$, $-16 \le l \le 15$	$-13 \le h \le 13$, $-28 \le k \le 28$, $-16 \le l \le 16$	$-10 \le h \le 10$, $-11 \le k \le 11$, $0 \le l \le 15$	$-10 \le h \le 11$, $-13 \le k \le 13$, $0 \le l \le 16$
reflections collected	24070	36616		8195
independent reflections [R(int)]	6397 [R(int) = 0.0501]	6551 [R(int) = 0.0350]	3890	8195
completeness to θ = 27.50/60.750/25.242/25.242°	100.0	99.2	96.5	99.7
absorption correction	semiempirical from equivalents	semiempirical from equivalents	semiempirical from equivalents	semiempirical from equivalents
max and min transmission	0.7456 and 0.6393	0.7456 and 0.6663	0.461 and 0.146	0.746 and 0.632
refinement method	full-matrix least-squares on F^2	full-matrix least-squares on F^2	full-matrix least-squares on F^2	full-matrix least-squares on F^2
data/restraints/parameters	6397/0/352	6551/0/361	3890/0/352	8195/31/300
goodness-of-fit on F^2	1.059	1.216	1.045	1.045
final R indices [$I > 2\sigma(I)$]	$R1$ = 0.0334, $wR2$ = 0.0669	$R1$ = 0.0382, $wR2$ = 0.0905	$R1$ = 0.0504, $wR2$ = 0.1308	$R1$ = 0.0230, $wR2$ = 0.0587
R indices (all data)	$R1$ = 0.0511, $wR2$ = 0.0740	$R1$ = 0.0411, $wR2$ = 0.0917	$R1$ = 0.0639, $wR2$ = 0.1378	$R1$ = 0.0243, $wR2$ = 0.0596
largest diff. peak and hole (e·Å^{-3})	0.960 and −0.512	0.800 and −0.730	1.592 and −0.947	0.630 and −0.468

Table 3. Selected Bond Lengths (Å) and Angles (deg) for Complexes 1−3 and 7

	1	2	3	7
Ru(1)−arene centroid	1.654	1.666	1.655	1.665
Ru(1)−Cl(1)	2.4006(6)	2.4404(6)	2.4160(8)	2.4180(6)
Ru(1)−N(1)	2.1352(16)	2.081(2)	2.081(2)	2.1009(17)
Ru(1)−N(3)/Ru(1)−O(1)/Ru(1)−O(1)/Ru(1)−O(1)	2.1017(17)	2.0719(16)	2.072(2)	2.0986(15)
Ru(1)−C(19)/C(25)/C(28)/C(25)	2.1654(19)	2.208(3)	2.188(3)	2.159(2)
Ru(1)−C(20)/C(20)/C(27)/C(20)	2.197(2)	2.174(3)	2.197(3)	2.197(2)
Ru(1)−C(21)/C(21)/C(26)/C(21)	2.189(2)	2.157(3)	2.183(3)	2.198(2)
Ru(1)−C(22)/C(22)/C(25)/C(22)	2.179(2)	2.165(2)	2.165(3)	2.189(2)
Ru(1)−C(23)	2.173(2)	2.189(2)	2.170(3)	2.185(2)
Ru(1)−C(24)	2.151(2)	2.154(3)	2.211(3)	2.173(2)
N(1)−Ru(1)−Cl(1)	85.50(5)	84.22(6)	84.22(6)	85.42(5)
N(3)−Ru(1)−Cl(1)/O(1)−Ru(1)−Cl(1)	85.39(5)	84.85(5)	84.85(5)	85.76(4)
N(3)−Ru(1)−N(1)/O(1)−Ru(1)−N(1)	61.53(6)	86.01(7)	86.01(7)	84.92(6)

hallmark of apoptosis.[54] The mechanism of cell death was analyzed using flow cytometry and by fluorescent staining methods. Complexes **2** and **3**, which showed efficient cytotoxic activity, were used for the flow cytometric analysis. The flow cytometry is one of the efficient and specific methods to investigate the molecular and morphological events occurring during cell death. The fractions of cell populations in different quadrants were analyzed using quadrant statistics. The lower left quadrant (R2), lower right quadrant (R3), upper right quadrant (R4), and upper left quadrant (R5) contained the living cells, early apoptosis cells, late apoptosis cells, and dead cells, respectively. From this, we could infer that the complexes induced apoptosis in accordance with their activity. The population of living cells decreased, and that of the early and late apoptotic cells increased after treatment with the complexes in HepG2 cells. In the case of complex **2**, 3.2% of

DOI: 10.1021/acs.organomet.8b00702
Organometallics XXXX, XXX, XXX−XXX

Table 4. Selected Bond Lengths (Å) and Angles (deg) for Complexes 4−6

	4	5	6
Ru(1)−arene centroid	1.659	1.660	1.662
Ru(2)−arene centroid	1.659	1.661	1.672
Ru(1)−Cl(1)	2.4388(9)	2.4410(11)	2.4218(18)
Ru(1)−N(2)/N(1)/N(1)	2.088(3)	2.084(3)	2.080(6)
Ru(1)−O(1)	2.083(2)	2.075(3)	2.056(6)
Ru(2)−Cl(2)	2.3916(9)	2.3984(10)	2.4055(19)
Ru(2)−N(1)/N(2)/N(2)	2.150(2)	2.164(3)	2.225(7)
Ru(2)−N(3)	2.068(2)	2.064(3)	2.073(7)
Ru(1)−C(19)/C(25)/C(19)	2.171(3)	2.175(4)	2.176(8)
Ru(1)−C(20)/C(26)/C(20)	2.162(3)	2.214(4)	2.168(8)
Ru(1)−C(21)/C(21)/C(21)	2.169(3)	2.170(4)	2.187(8)
Ru(1)−C(22)	2.164(3)	2.183(5)	2.201(8)
Ru(1)−C(23)	2.209(3)	2.158(4)	2.187(8)
Ru(1)−C(24)	2.163(3)	2.174(4)	2.188(8)
Ru(2)−C(25)/C(31)/C(25)	2.153(3)	2.191(5)	2.175(8)
Ru(2)−C(26)/C(32)/C(26)	2.213(3)	2.210(5)	2.203(10)
Ru(2)−C(27)	2.174(3)	2.146(5)	2.163(10)
Ru(2)−C(28)	2.177(4)	2.170(5)	2.148(9)
Ru(2)−C(29)	2.140(4)	2.159(4)	2.129(9)
Ru(2)−C(30)	2.151(4)	2.180(4)	2.169(9)
O(1)−Ru(1)−Cl(1)	86.26(7)	85.88(9)	86.67(17)
O(1)−Ru(1)−N(2)/N(1)/N(1)	85.00(9)	84.17(12)	85.0(2)
N(2)/N(1)/N(1)−Ru(1)−Cl(1)	83.98(7)	84.53(10)	84.52(17)
N(1)/N(2)/N(2)−Ru(2)−Cl(2)	86.11(7)	85.76(9)	83.73(18)
N(3)−Ru(2)−Cl(2)	85.68(7)	85.40(10)	85.06(19)
N(3)−Ru(2)−N(1)/N(2)/N(2)	61.66(10)	61.61(13)	60.1(3)

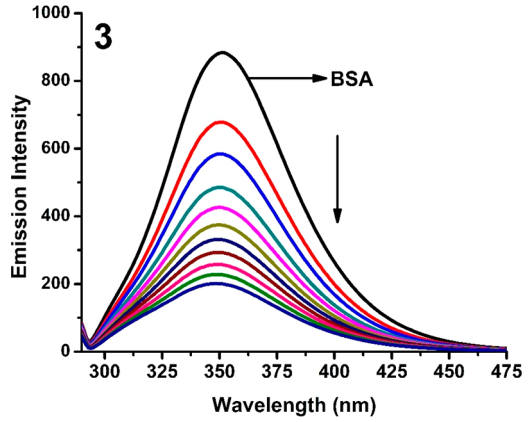

Figure 10. Fluorescence quenching curves of BSA in the absence and presence of **3**. [BSA] = 1 μM and [complex] = 0−20 μM.

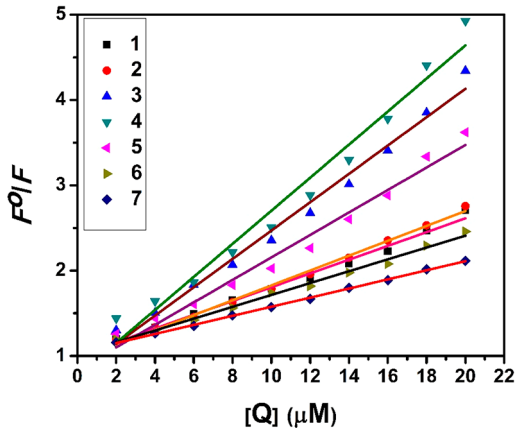

Figure 11. Stern−Volmer plot of the fluorescence titrations of the complexes with BSA.

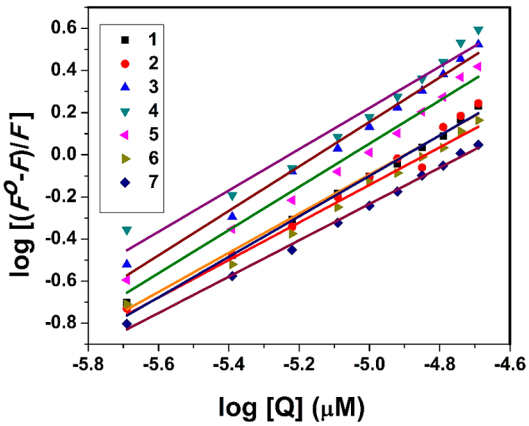

Figure 12. Scatchard plot of the fluorescence titrations of the complexes with BSA.

Table 5. Protein Binding Constant (K_b), Quenching Constant (K_q), and Number of Binding Sites (n) for Complexes 1−7

complex	K_b (M^{-1})	K_q (M^{-1})	n
1	3.54×10^4	8.07×10^4	0.92
2	5.06×10^4	8.71×10^4	0.96
3	2.72×10^5	1.66×10^5	1.05
4	1.32×10^5	1.31×10^5	0.98
5	1.51×10^5	1.93×10^5	1.02
6	2.06×10^4	6.94×10^4	0.89
7	1.20×10^4	5.33×10^4	0.86

early apoptosis and 58.5% late apoptosis were observed. Complex **3** induced 15.4% early apoptosis and 69.5% late apoptosis (Figure 18).

The mode of cell death was visualized using fluorescent staining method. HepG2 and A549 cells treated with IC_{50} concentration of complexes **2** (HepG2, 9.33 μg/mL, and A549, 62.5 μg/mL) and **3** (HepG2, 10.89 μg/mL) were subjected to confocal microscopic studies. In this study, 4′,6-diamidino-2-phenylindole (DAPI, blue), fluorescein isothiocyanate (FITC, green), and propidium iodide (PI) fluorescence (red) stains were used to assess the morphological changes in the cell after treatment with the complexes. DAPI bound strongly to A-T-rich regions in DNA and passed through an intact cell membrane. FITC acted as a phosphatidyl serine tracer and suggested the presence of apoptosis. PI could only penetrate cells where the cell membrane had been compromised. The results showed that significant morphological changes like condensation and fragmentation were found after treatment of the complexes with HepG2 and A549 cells, and apoptotic cells were indicated with arrows in Figures 19 and 20.

CONCLUSIONS

We have accomplished the synthesis of novel Ru(II)−arene complexes containing guanidine ligands which exhibited versatile coordination behavior to form monometallic (N,N/

DOI: 10.1021/acs.organomet.8b00702
Organometallics XXXX, XXX, XXX−XXX

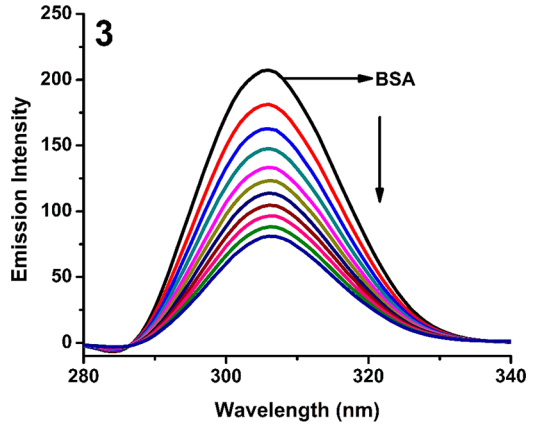

Figure 13. Synchronous spectra of BSA (1 μM) as a function of concentration of **3** (0−20 μM) with $\Delta\lambda$ = 15 nm.

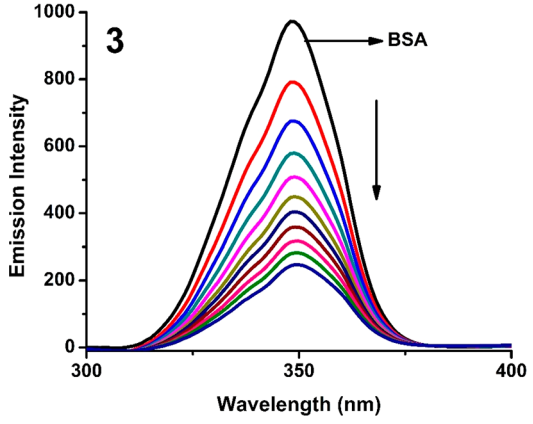

Figure 14. Synchronous spectra of BSA (1 μM) as a function of concentration of **3** (0−20 μM) with $\Delta\lambda$ = 60 nm.

Table 6. In Vitro Cytotoxic Activity of the Complexes in HepG2, A549, and Vero Cell Lines

	IC_{50} (μM)		
complex	HepG2	A549	Vero
1	>250	176.33	>250
2	15.41	58.18	136.98
3	17.74	128.78	152.33
4	>250	>250	>250
5	>250	>250	>250
6	>250	>250	>250
7	59.01	143.85	>250
cisplatin	21.5	18	

N,O) Ru−*p*-cymene complexes and monometallic (O,N) and bimetallic (N,N and N,O) Ru−benzene complexes. The complexes were characterized by various spectroscopic and X-ray crystallographic techniques. The binding efficacy of the complexes to DNA has been investigated using spectroscopic and hydrodynamic measurements. The intrinsic binding constant revealed that the Ru−*p*-cymene complexes showed higher binding ability than the Ru−benzene analogues. The spectroscopic evidence also supported the binding of the complexes to BSA. The in vitro cytotoxic studies revealed that the complexes with the N,O bidentate ligand showed appreciable activity than the N,N-type complexes against two cancer cell lines. Complexes **2** and **3** were the most active against HepG2 cell line; interestingly, **2** was more efficient than cisplatin. The cell death mechanism of the active complexes **2** and **3** was found to be apoptosis as assessed by flow cytometry and staining methods. The active complexes which showed appreciable binding ability with biomolecules and possessed remarkable cytotoxic activity might be a potential anticancer drug.

EXPERIMENTAL SECTION

Materials and Methods. Chemicals obtained from commercial suppliers were used as received and were of analytical grade. The melting points were determined on Lab India instrument and are uncorrected. Elemental analyses were carried out using PerkinElmer instrument. FT-IR spectra were obtained as KBr pellets using a Nicolet-iS5 spectrophotometer. UV−visible spectra were recorded using a Shimadzu-2600 spectrophotometer. Emission spectra were measured on a Jasco V-630 spectrophotometer using 5% DMF in buffer as the solvent. NMR spectra were recorded in $CDCl_3$/DMSO-d_6 solvent using TMS as an internal standard on a Bruker 500/400 MHz spectrometer. ESI-MS spectra were recorded using a high resolution Bruker maXis impact mass spectrometer.

Synthesis of the Ligands. The ligands **L1**−**L4** were described previously.[24−26] The guanidine ligand (**L5**) was synthesized from *N*-furoyl-*N*′-phenylthiourea by guanylation method.[55] Thiourea (0.2462 g, 5 mmol) was mixed with aniline (0.456 mL, 5 mmol) in DMF and triethylamine (1 mL, 10 mmol). The temperature was maintained below 5 °C using an ice bath, and 1 equiv of mercuric chloride (1.3576 g, 5 mmol) was added to the reaction mixture with vigorous stirring. The ice bath was removed after 30 min, and the stirring was continued overnight. The progress of the reaction was monitored using TLC. After all the thiourea was consumed, 20 mL of chloroform was added to the reaction mixture and the suspension was filtered through a sintered glass funnel to remove the HgS residue. The solvents were evaporated under reduced pressure, and the solid residue was dissolved in 20 mL of CH_2Cl_2, then washed with water, and the organic phase was dried over anhydrous Na_2SO_4. The residue obtained after evaporation of the solvent was recrystallized from ethanol to get the crystals of **L5**.

N,N′*-Diphenyl-N*″*-furoylguanidine (**L5**).* Yield: 63%, white solid; mp 120 °C. Anal. Calcd for $C_{18}H_{15}N_3O_2$: C, 70.81; H, 4.95; N, 13.76. Found: C, 70.65; H, 5.14; N, 13.60. ESI-MS (m/z): found 306.1262 $(M + H)^+$; calcd for $C_{18}H_{15}N_3O_2$ 305.1164. UV−vis (ethanol): λ, nm (ε, $dm^3\ mol^{-1}\ cm^{-1}$) 295 (20850), 286 (20400). FT-IR (KBr, cm^{-1}): 3395, 3226 (N−H), 1590 (C═O), 1558 (C═N). ^{1}H NMR (500 MHz, $CDCl_3$): δ, ppm 10.06 (s, 1H), 8.39 (s, 1H), 7.74−7.69 (m, 2H), 7.63−7.53 (m, 1H), 7.42 (d, J = 8.1 Hz, 3H), 7.24 (d, J = 7.9 Hz, 2H), 7.17−7.01 (m, 4H), 6.50 (d, J = 12.4 Hz, 1H). ^{13}C NMR (125 MHz, $CDCl_3$): δ, ppm 169.6 (C═O), 156.4 (C═N), 152.3, 145.9, 145.3, 137.2, 136.4, 129.8, 129.5, 128.9, 126.0, 124.1, 115.8, 111.6 (aromatic carbons).

Synthesis of the Ru−Arene Complexes. The ligand **L1** (1 mmol) and NaOMe (0.054 g, 1 mmol) were dissolved in methanol (20 mL) and stirred for 30 min at room temperature. Then $[RuCl(\mu\text{-}Cl)(\eta^6\text{-}p\text{-cymene})]_2$ (0.6120 g, 1 mmol) was added, which turned the reaction mixture into a red solution. After 6 h of reflux, the clear red solution was evaporated to dryness, and the residue was dissolved in chloroform, from which the precipitate was slowly formed, which was filtered off and dried. Recrystallization of the crude product with methanol yielded reddish orange crystals (**1**). For the synthesis of complexes **2** and **3** from **L2** and **L3**, respectively, the same procedure was followed except the reaction mixture was stirred at reflux for 8−10 h.

The ligands **L1**/**L2**/**L4**/**L5** (1 mmol) and NaOMe (0.054 g, 1 mmol) were dissolved in methanol (20 mL) and stirred for 30 min at room temperature. Addition of $[RuCl(\mu\text{-}Cl)(\eta^6\text{-benzene})]_2$ (0.5000 g, 1 mmol) to the above solution turned it red. After 6 h of stirring at room temperature, an orange solid appeared. The solid was filtered off, washed with methanol, and dried in vacuo. The solid was

DOI: 10.1021/acs.organomet.8b00702
Organometallics XXXX, XXX, XXX−XXX

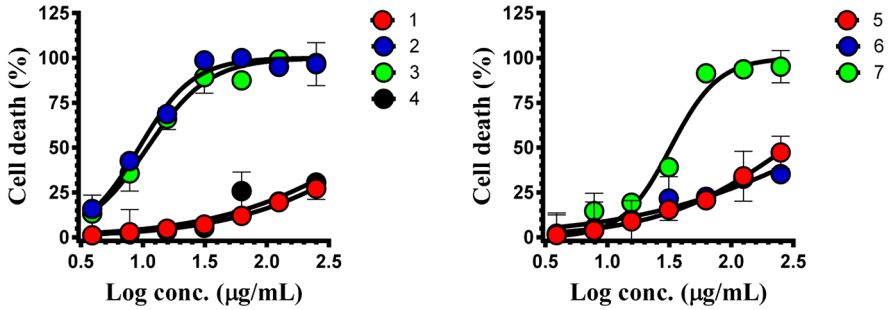

Figure 15. Comparison of cytotoxic activity of complexes **1**−**7** against HepG2 cancer cells (24 h exposure). Data were calculated by mean ± SD of three independent experiments with each experiment conducted in triplicate.

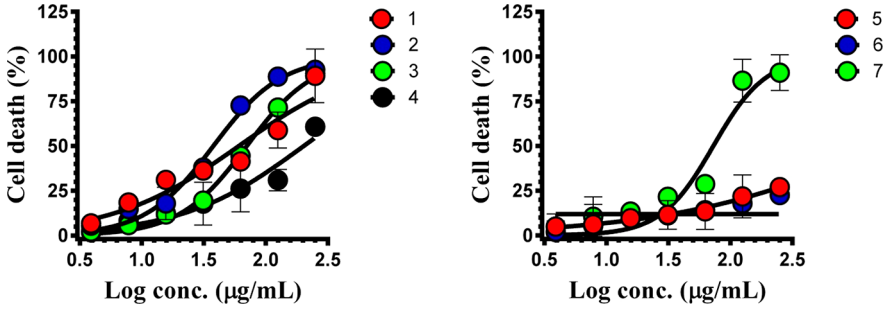

Figure 16. Comparison of cytotoxic activity of complexes **1**−**7** against A549 cancer cells (24 h exposure). Data were calculated by mean ± SD of three independent experiments with each experiment conducted in triplicate.

recrystallized in methanol/chloroform mixture to get red crystals (**4**−**7**).

*[RuCl(η^6-p-cymene)(**L1**-N,N)] (**1**).* **L1** (0.3213 g, 1 mmol) was used. Yield: 79%, orange solid; mp 185 °C. Anal. Calcd for $C_{28}H_{28}ClN_3ORuS$: C, 56.89; H, 4.77; N, 7.11; S, 5.42. Found: C, 56.73; H, 4.58; N, 7.29; S, 5.61. ESI-MS (m/z): found 556.0997 (M − Cl)$^+$; calcd for $C_{28}H_{28}ClN_3ORuS$ 591.0685. UV−vis (ethanol): λ, nm (ε, dm^3 mol^{-1} cm^{-1}) 248 (32700), 292 (25200), 439 (1446). FT-IR (KBr, cm^{-1}): 3203 (N−H), 1610 (C═O), 1559 (C═N). ^{1}H NMR (500 MHz, $CDCl_3$): δ, ppm 10.32 (s, 1H), 8.47 (d, J = 1.1 Hz, 1H), 7.53 (d, J = 4.7 Hz, 1H), 7.47−7.42 (m, 1H), 7.14 (t, J = 8.9 Hz, 1H), 6.96 (d, J = 3.4 Hz, 3H), 6.86 (t, J = 7.5 Hz, 3H), 6.74 (t, J = 7.3 Hz, 1H), 6.69 (d, J = 7.8 Hz, 2H), 5.09−5.00 (m, 4H, *p*-cymene phenyl-H), 2.63−2.58 (m, 1H, *p*-cymene C**H**$(CH_3)_2$), 2.34 (s, 3H, *p*-cymene CH_3), 1.22 (d, J = 5.8 Hz, 6H, *p*-cymene CH$(CH_3)_2$). ^{13}C NMR (125 MHz, $CDCl_3$): δ, ppm 170.3 (C═O), 155.62 (C═N), 145.2, 141.7, 135.4, 132.0, 130.2, 128.0, 127.9, 126.9, 124.0, 123.7, 122.8, 122.3 (aromatic carbons), 100.6, 98.5, 81.3, 80.8 (aromatic carbons of *p*-cymene), 31.2, 22.4, 19.0 (aliphatic carbons in *p*-cymene).

*[RuCl(η^6-p-cymene)(**L2**-O,N)] (**2**).* **L2** (0.3354 g, 1 mmol) was used. Yield: 76%, orange solid; mp 174 °C. Anal. Calcd for $C_{29}H_{30}ClN_3ORuS$: C, 57.56; H, 5.00; N, 6.94; S, 5.30. Found: C, 57.71; H, 5.19; N, 6.79; S, 5.47. ESI-MS (m/z): found 570.1160 (M − Cl)$^+$; calcd for $C_{29}H_{30}ClN_3ORuS$ 605.0842. UV−vis (ethanol): λ, nm (ε, dm^3 mol^{-1} cm^{-1}) 252 (18300), 289 (15700), 434 (1102). FT-IR (KBr, cm^{-1}): 3417 (N−H), 1571 (C═O), 1532 (C═N). ^{1}H NMR (500 MHz, $CDCl_3$): δ, ppm 8.85 (t, J = 5.7 Hz, 1H), 8.43 (dd, J = 3.6, 1.1 Hz, 1H), 7.73 (dd, J = 3.6, 1.1 Hz, 1H), 7.48 (dd, J = 4.9, 1.1 Hz, 1H), 7.43 (dd, J = 8.4, 7.5 Hz, 1H), 7.31 (dd, J = 5.0, 1.1 Hz, 1H), 7.24−7.22 (m, 2H), 7.18−7.16 (m, 2H), 7.12−7.08 (m, 1H), 7.02 (d, J = 6.6 Hz, 1H), 6.98 (dd, J = 5.0, 3.7 Hz, 1H), 5.14−4.93 (m, 7H, *p*-cymene phenyl-H, NH, CH_2), 2.73−2.66 (m, 1H, *p*-cymene C**H**$(CH_3)_2$), 2.21 (s, 3H, *p*-cymene CH_3), 1.18 (d, J = 6.9 Hz, 6H, *p*-cymene CH$(CH_3)_2$). ^{13}C NMR (125 MHz, $CDCl_3$): δ, ppm 175.7 (C═O), 159.1 (C═N), 155.4, 146.8, 142.2, 140.0, 137.1, 131.9, 130.1, 129.7, 128.4, 128.3, 127.3, 127.1, 127.1, 126.7, 125.8, 124.6 (aromatic carbons), 101.5, 97.9, 83.7, 80.4 (aromatic carbons of *p*-cymene), 46.6 (aliphatic carbon in the ligand), 30.9, 21.9, 18.3 (aliphatic carbons in *p*-cymene).

*[RuCl(η^6-p-cymene)(**L3**-O,N)] (**3**).* **L3** (0.3434 g, 1 mmol) was used. Yield: 76%, orange solid; mp 185 °C. Anal. Calcd for $C_{32}H_{34}ClN_3ORu$: C, 62.68; H, 5.59; N, 6.85. Found: C, 62.52; H, 5.77; N, 6.66. ESI-MS (m/z): found 577.1554 (M − Cl)$^+$; calcd for $C_{32}H_{34}ClN_3ORu$ 613.1434. UV−vis (ethanol): λ, nm (ε, dm^3 mol^{-1} cm^{-1}) 250 (31300), 319 (9200), 441 (1033). FT-IR (KBr, cm^{-1}): 3419 (N−H), 1593 (C═O), 1566 (C═N). ^{1}H NMR (500 MHz, $CDCl_3$): δ, ppm 8.20 (d, J = 4.3 Hz, 2H), 7.45 (d, J = 10.1 Hz, 3H), 7.37−7.17 (m, 4H), 7.14 (d, J = 5.0 Hz, 2H), 7.04 (t, J = 10.1 Hz, 3H), 5.30−3.89 (m, 7H, *p*-cymene phenyl-H, NH, CH_2), 2.60−2.52 (m, 1H, *p*-cymene C**H**$(CH_3)_2$), 2.31 (s, 3H, *p*-cymene CH_3), 2.15 (s, 3H), 1.14 (dd, J = 28.6, 4.0 Hz, 6H, *p*-cymene CH$(CH_3)_2$). ^{13}C NMR (125 MHz, $CDCl_3$): δ, ppm 176.6 (C═O), 159.4 (C═N), 143.8, 137.3, 134.1, 130.2, 129.2, 129.0, 128.45, 127.61, 127.2, 124.4 (aromatic carbons), 99.9, 97.9, 81.0, 79.1 (aromatic carbons of *p*-cymene), 46.7 (aliphatic carbon in the ligand), 31.0, 22.6 (aliphatic carbons in *p*-cymene), 21.0 (aliphatic carbon in the ligand), 18.9 (aliphatic carbons in *p*-cymene).

*[{Ru(η^6-C_6H_6)Cl}$_2$(**L1**-N,N,O,N)] (**4**).* **L1** (0.3213 g, 1 mmol) was used. Yield: 76%, orange solid; mp 295 °C. Anal. Calcd for $C_{30}H_{25}Cl_2N_3ORu_2S$: C, 48.13; H, 3.37; N, 5.61; S, 4.28. Found: C, 48.32; H, 3.51; N, 5.46; S, 4.48. ESI-MS (m/z): found 500.0372 [M − 2Cl − Ru(η^6-C_6H_6)]$^+$; calcd for $C_{30}H_{25}Cl_2N_3ORu_2S$ 748.9182. UV−vis (DMF): λ_{max}, nm (ε, dm^3 mol^{-1} cm^{-1}) 250 (11900), 269 (11757), 452 (1457). FT-IR (KBr, cm^{-1}): 1592 (C═O), 1543 (C═N). ^{1}H NMR (400 MHz, $CDCl_3$): δ, ppm 8.57 (dd, J = 3.7, 1.1 Hz, 1H), 7.46 (dd, J = 4.9, 1.1 Hz, 2H), 7.03 (dd, J = 4.9, 3.7 Hz, 2H), 6.82−6.77 (m, 6H), 6.66 (t, J = 7.3 Hz, 1H), 6.59 (t, J = 7.3 Hz, 1H), 5.11 (s, 6H, benzene), 4.95 (s, 6H, benzene). ^{13}C NMR (100 MHz, $CDCl_3$): δ, ppm 166.1 (C═O), 159.5 (C═N), 157.7, 152.9, 152.0, 148.5, 144.5, 139.9, 132.0, 130.9, 130.0, 129.5, 127.4, 126.8, 126.5, 125.2, 123.6, 123.5, 123.0 (aromatic carbons), 83.7, 82.7 (aromatic carbons of benzene).

*[{Ru(η^6-C_6H_6)Cl}$_2$(**L4**-N,N,O,N)] (**5**).* **L4** (0.3153 g, 1 mmol) was used. Yield: 70%, orange solid; mp 290 °C. Anal. Calcd for $C_{32}H_{27}Cl_2N_3ORu_2$: C, 51.75; H, 3.66; N, 5.66. Found: C, 51.91; H, 3.81; N, 5.83. ESI-MS (m/z): found 494.0798 [M − 2Cl − Ru(η^6-

DOI: 10.1021/acs.organomet.8b00702
Organometallics XXXX, XXX, XXX−XXX

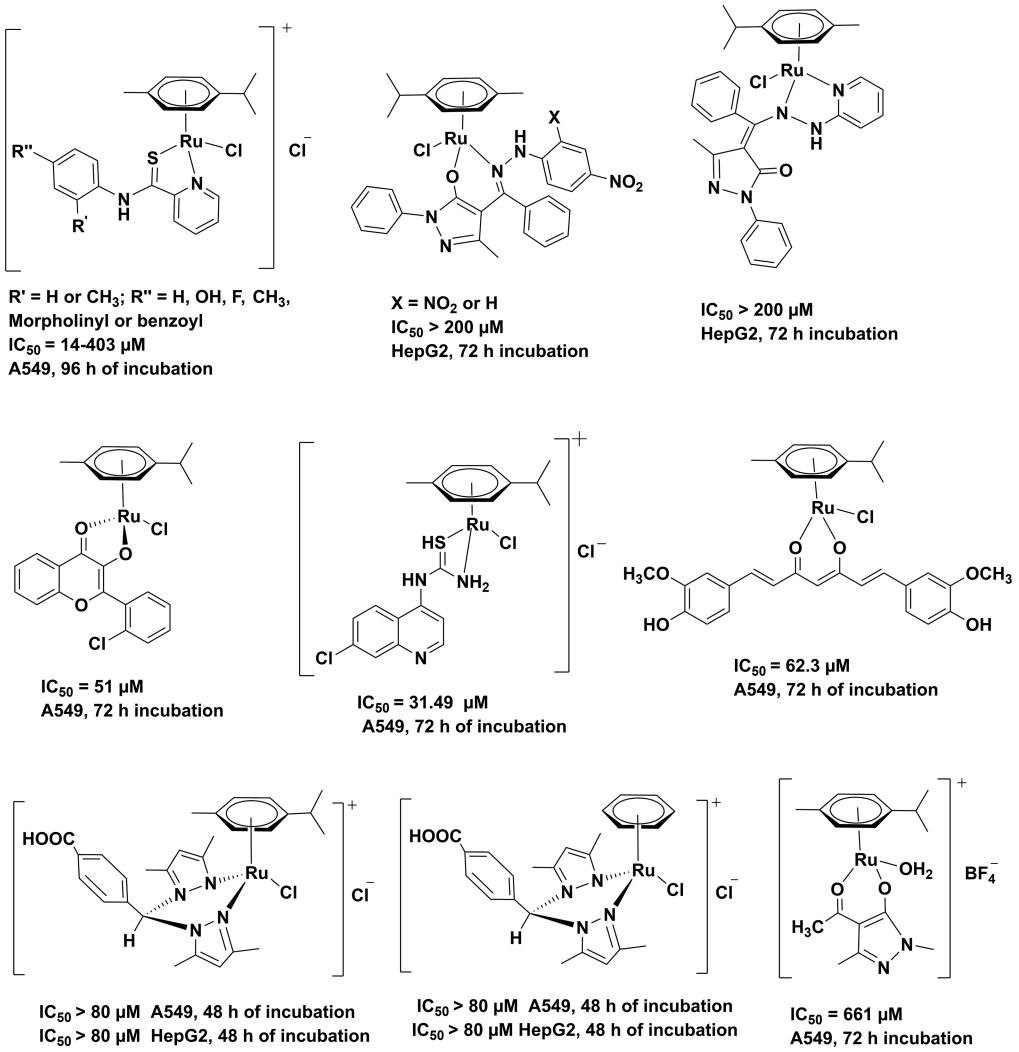

Figure 17. IC_{50} values of reported [RuCl(η^6-arene)L]-type complexes (L is a bidentate ligand).

$C_6H_6)]^+$; calcd for $C_{32}H_{27}Cl_2N_3ORu_2$ 742.9618. UV−vis (DMF): λ_{max}, nm (ε, $dm^3\ mol^{-1}\ cm^{-1}$) 243 (9785), 334 (3100), 454 (1128). FT-IR (KBr, cm^{-1}) 1594 (C═O), 1552 (C═N). ^1H NMR (500 MHz, DMSO-d_6): δ, ppm 8.18 (d, J = 3.9 Hz, 1H), 7.60 (d, J = 12.0 Hz, 2H), 7.43−7.21 (m, 4H), 7.00−6.45 (m, 8H), 5.98 (s, 12H, benzene). ^{13}C NMR (125 MHz, $CDCl_3$): δ, ppm 176.6 (C═O), 156.1 (C═N), 144.9, 138.2, 135.2, 130.7, 129.0, 128.1, 128.0, 127.8, 124.4, 123.8, 122.7, 122.6 (aromatic carbons), 82.3 (aromatic carbons of benzene).

*[{Ru(η^6-C_6H_6)Cl}$_2$(**L5**-N,N,O,N)] (**6**).* **L5** (0.3053 g, 1 mmol) was used. Yield: 66%, orange solid; mp 275 °C. Anal. Calcd for $C_{30}H_{25}Cl_2N_3O_2Ru_2$: C, 49.18; H, 3.44; N, 5.74. Found: C, 49.02; H, 3.63; N, 5.90. ESI-MS (m/z): Found 484.0583 [M − 2Cl − Ru(η^6-C_6H_6)]$^+$; calcd for $C_{30}H_{25}Cl_2N_3O_2Ru_2$ 732.9411. UV−vis (DMF): λ_{max}, nm (ε, $dm^3\ mol^{-1}\ cm^{-1}$) 268 (18850), 332 (7975), 451 (1775). FT-IR (KBr, cm^{-1}): 1579 (C═O), 1544 (C═N). ^1H NMR (400 MHz, DMSO-d_6): δ 8.47 (d, J = 3.6 Hz, 1H), 8.09 (d, J = 5.0 Hz, 1H), 8.02 (d, J = 9.1 Hz, 1H), 7.98 (d, J = 9.1 Hz, 2H), 7.95 (d, J = 8.3 Hz, 2H), 7.63−7.57 (m, 3H), 7.32−7.28 (m, 3H), 5.98 (s, 12H, benzene). ^{13}C NMR (100 MHz, DMSO-d_6): δ, ppm 180.7 (C═O), 162.2 (C═N), 136.7, 135.3, 134.2, 133.7, 132.7, 128.7, 128.6, 128.3, 128.3, 127.3, 126.7, 126.3, 125.4, 124.6, 122.2 (aromatic carbons), 87.6 (aromatic carbons of benzene).

*[RuCl(η^6-C_6H_6)(**L2**-N,O)] (**7**).* **L2** (0.3354 g, 1 mmol) was used. Yield: 66%, reddish brown solid; mp 301 °C. Anal. Calcd for $C_{25}H_{22}ClN_3ORuS$: C, 54.69; H, 4.04; N, 7.65; S, 5.84. Found: C, 54.87; H, 4.24; N, 7.46; S, 5.99. UV−vis (DMF): λ_{max}, nm (ε, $dm^3\ mol^{-1}\ cm^{-1}$) 244 (8400), 294 (5542), 422 (971). FT-IR (KBr): ν, cm^{-1} 3419 (N−H), 1561(C═O), 1526 (C═N). ^1H NMR (500 MHz, DMSO-d_6): δ, ppm δ 8.18 (d, J = 3.9 Hz, 1H), 7.60 (d, J = 12.7 Hz, 2H), 7.44−7.08 (m, 4H), 6.96−6.45 (m, 6H), 5.98 (s, 6H, benzene), 5.28 (s, 1H), 4.83 (s, 2H). ^{13}C NMR (125 MHz, DMSO-d_6): δ, ppm 164.2 (C═O), 158.0 (C═N), 155.0, 141.8, 131.1, 130.1, 128.8, 128.4, 127.9, 126.7, 121.5, 116.8 (aromatic carbons), 88.1 (aromatic carbon of benzene), 45.9 (aliphatic carbon in the ligand).

Solubility Measurements. The concentrations of saturated solutions of the Ru(II) complexes were determined by UV−visible studies by following a literature procedure.[56]

Stability Studies. The stability of complexes **1**−**7** in 1% DMSO/water mixture was monitored over a period of 24 h by UV−visible spectroscopy. The complexes which were stable in a 1% DMSO/water mixture were monitored for their stability in biological medium. The test was done by dissolving the complexes in minimum quantity of 1% DMSO, and it was diluted with PBS buffer. The UV−visible spectra of the resultant mixture were monitored over a period of 24 h.

X-ray Crystallography. A Bruker APEX2 [or GADDS (for **2** and **6**)] X-ray (three-circle) diffractometer was employed for crystal screening, unit cell determination, and data collection. Integrated intensity information for each reflection was obtained by reduction of the data frames with the program APEX2.[57] The integration method employed a three-dimensional profiling algorithm, and all data were corrected for Lorentz and polarization factors, as well as for crystal decay effects. Finally, the data were merged and scaled to produce a suitable data set. The absorption correction program SADABS[58] [or

DOI: 10.1021/acs.organomet.8b00702
Organometallics XXXX, XXX, XXX−XXX

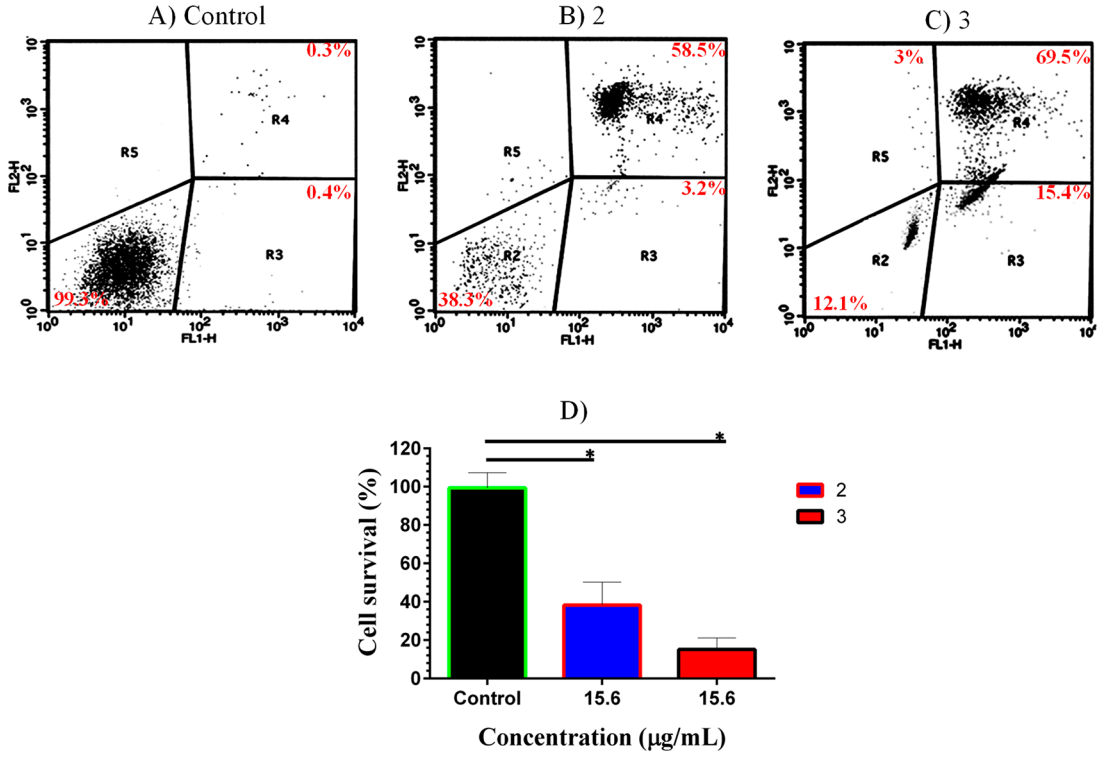

Figure 18. Apoptosis of HepG2 cells treated with IC_{50} concentrations (15.63 μg/mL) of **2** and **3** for 24 h. The percentage of apoptotic cells was determined by flow cytometry. Values are the mean ± SD from at least three independent experiments. Significance was calculated by Tukey's multiple comparisons test (n = 3); *p < 0.05 indicates the significant differences from the control. The four areas in the diagrams represent four different cell states: living cells (R2), early apoptotic cells (R3), late apoptotic cells (R4), and dead cells (R5).

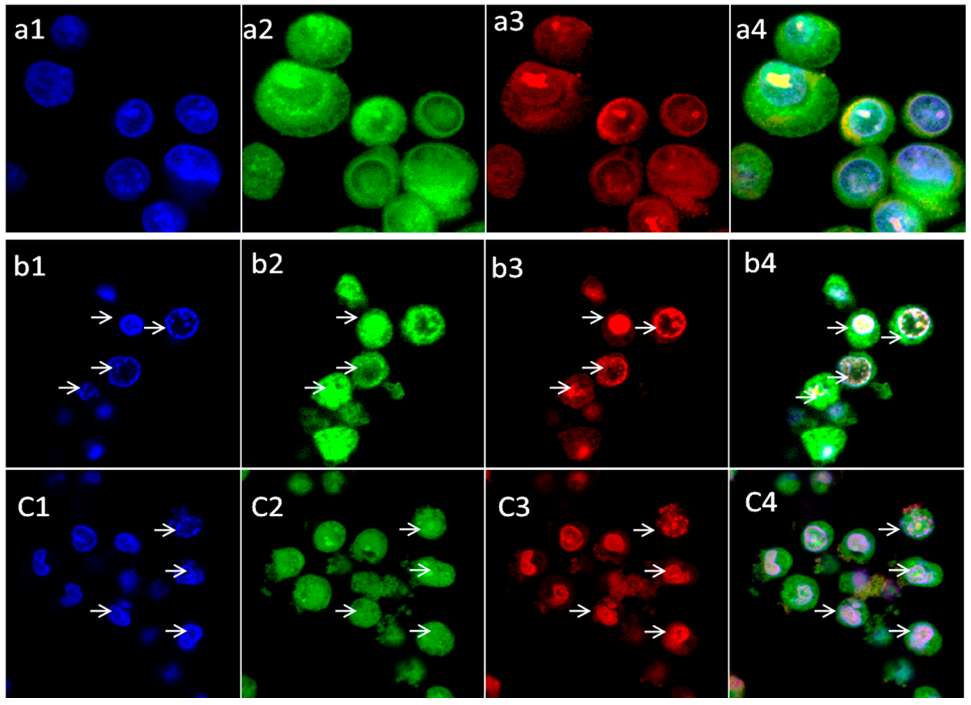

Figure 19. DAPI (blue), FITC (green), and PI (red) fluorescence staining for the detection of apoptosis in HepG2 cells. Cells were treated with complexes **2** and **3** at the IC_{50} concentration of 15.6 μg/mL. The fluorescent signals of DAPI, FITC, and PI were examined under a confocal laser scanning microscope. Control: a1-DAPI, a2-FITC, a3-PI, and a4-merged. Treated: **2** b1-DAPI, b2-FITC, b3-PI, and b4-merged; **3** c1-DAPI, c2-FITC, c3-PI, and c4-merged. Arrows indicate apoptotic cancer cells.

TWINABS[58] (for **6** and **7**)] was employed to correct the data for absorption effects. Systematic reflection conditions and statistical tests of the data suggested the space group. Solutions were obtained readily using SHELXT (XT).[59,60] Hydrogen atoms were placed in idealized positions and were set riding on the respective parent atoms. All non-hydrogen atoms were refined with anisotropic thermal parameters.

DOI: 10.1021/acs.organomet.8b00702
Organometallics XXXX, XXX, XXX−XXX

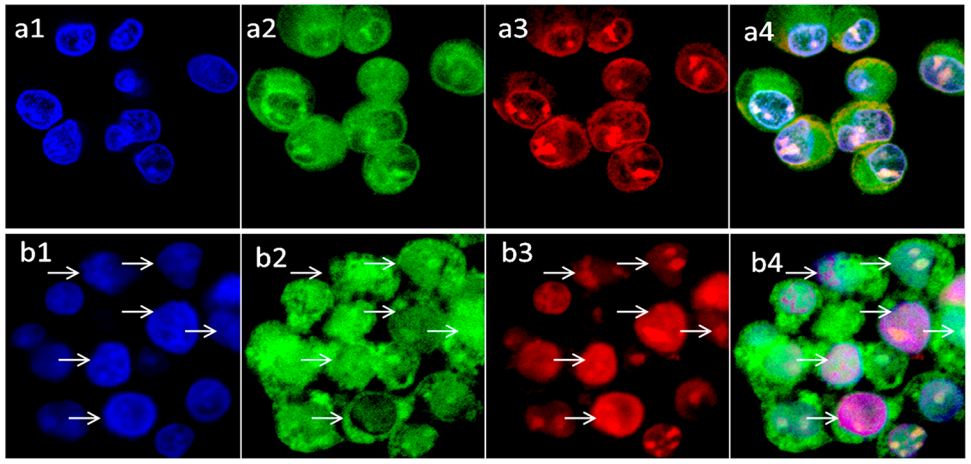

Figure 20. DAPI (blue), FITC (green), and PI (red) fluorescence staining for the detection of apoptosis in A549 cells. Cells were treated with complex **2** at the IC_{50} concentration of 62.5 μg/mL. The fluorescent signals of DAPI, FITC, and PI were examined under a confocal laser scanning microscope. Control: a1-DAPI, a2-FITC, a3-PI, and a4-merged. Treated: **2** b1-DAPI, b2-FITC, b3-PI, and b4-merged. Arrows indicate apoptotic cancer cells.

The structures were refined (weighted least-squares refinement on F^2) to convergence.[58−61] Olex2 was employed for the final data presentation and structure plots.[61]

DNA Interaction Studies. The detailed experimental procedures for DNA binding studies by UV−visible, fluorescence, and viscosity measurements are given in the Supporting Information.

Protein Binding Studies. The binding of Ru−arene complexes **1**−**7** with BSA was studied using fluorescence spectra recorded at a fixed excitation wavelength corresponding to BSA at 280 nm and monitoring the emission at 335 nm. The excitation and emission slit widths and scan rates were constantly maintained for all the experiments. Stock solution of BSA was prepared in 50 mM phosphate buffer (pH 7.2) and stored in the dark at 4 °C for further use. Concentrated stock solutions of each test compound were prepared by dissolving it in DMF−phosphate buffer (5:95) and diluted with phosphate buffer to get required concentrations. Next, 2.5 mL of BSA solution was titrated by successive additions of the complexes (2 μM). For synchronous fluorescence spectra measurements, the same concentration of BSA and the complexes were used and the spectra were measured at two different $\Delta\lambda$ (difference between the excitation and emission wavelengths of BSA) values of 15 and 60 nm.

Cytotoxic Activity. Cytotoxic activity of the Ru(II)−arene complexes was studied against HepG2, A549, and Vero cell lines. The cells were maintained in Dulbecco's modified Eagle's medium with 10% fetal bovine serum and 2 mM L-glutamine, along with antibiotics (about 100 international unit/mL of penicillin, 100 μg/mL of streptomycin) with the pH adjusted to 7.2. One hundred microliters of medium containing 15000 cells/well and different concentrations of the complexes were seeded in 96-well plates. The complexes were dissolved in DMSO (10 mg/mL) to prepare stock solution for cytotoxic studies. The cells were cultivated at 37 °C with 5% CO_2 and 95% air in 100% relative humidity. After 24 h, an aliquot of 100 mL of medium containing 1 mg/mL of 3-(4,5-dimethylthiazol-2-yl)-2,5-diphenyltetrazolium bromide (MTT) was loaded into the plate. The cells were cultured for 4 h, and then the solution in the medium was removed. An aliquot of 100 μL of DMSO was added to the plate which was shaken until the crystals were dissolved.[62] The activity against cancer cells was determined by measuring the absorbance of the converted dye at 570 nm in an ELISA reader. Cytotoxicity of each sample was expressed as IC_{50} value. The percentage of growth inhibition was calculated using the following formula:

$$\frac{\text{mean OD of the untreated cells (control)} - \text{mean OD of the treated cells}}{\text{mean OD of the untreated cells (control)}} \times 100$$

Apoptosis Determination by Flow Cytometry. Apoptosis was analyzed using an Annexin V-FITC/PI detection kit (Biolegend, San Diego).[63] HepG2 cells were harvested after treatment and resuspended in binding buffer. Aliquots of 10^5 cells were mixed with 5 μL each of annexin V-FITC and PI solution for 15 min at room temperature in the dark. After incubation, 400 μL binding buffer was added, and cells were analyzed by FACS Calibur flow cytometer (Becton Dickinson).

Morphological Changes by Fluorescence Microscopy. HepG2 cells in the absence and presence of complexes **2** and **3** at IC_{50} concentration were used for confocal microscopic analysis. Similarly, the morphological changes in A549 cells with and without the addition of complex **2** (62.5 μg/mL) were viewed. After 24 h of treatment, cells were washed twice with 0.01 M PBS and suspended in binding buffer (ice-cold 1:1 methanol/acetone). Cells were incubated with DAPI, FITC, and PI for 30 min at 4 °C in the dark. Cells were then centrifuged, and pellets were smeared. DAPI, FITC, and PI fluorescence were immediately observed under confocal laser scanning microscope (ZEISS, LSM710, Germany).[64a,b]

■ ASSOCIATED CONTENT

Supporting Information

The Supporting Information is available free of charge on the ACS Publications website at DOI: 10.1021/acs.organomet.8b00702.

Figures depicting the graphs of stability/binding studies and NMR spectra of L5 and all of the complexes (PDF)

Accession Codes

CCDC 1491584−1491591 contain the supplementary crystallographic data for this paper. These data can be obtained free of charge via www.ccdc.cam.ac.uk/data_request/cif, or by emailing data_request@ccdc.cam.ac.uk, or by contacting The Cambridge Crystallographic Data Centre, 12 Union Road, Cambridge CB2 1EZ, UK; fax: +44 1223 336033.

DOI: 10.1021/acs.organomet.8b00702
Organometallics XXXX, XXX, XXX−XXX

AUTHOR INFORMATION

Corresponding Author

*E-mail: kar@nitt.edu.

ORCID

Chandrasekar Balachandran: 0000-0002-0750-2316

Ramasamy Karvembu: 0000-0001-8966-8602

Notes

The authors declare no competing financial interest.

ACKNOWLEDGMENTS

R.K. gratefully acknowledges SERB (EMR/2016/00321) for the financial support. K.J. thanks the Department of Science and Technology, Ministry of Science and Technology, Government of India for doctoral fellowship under DST-INSPIRE programme. J.H. thanks the University Grants Commission for the fellowship (F1-17.1/2012-13/RGNF-2012-13-ST-AND-18716). Authors sincerely thank Prof. N. Emi, Department of Hematology, Fujita Health University, Japan for cytotoxicity studies.

REFERENCES

(1) Jakupec, M. A.; Galanski, M.; Arion, V. B.; Hartinger, C. G.; Keppler, B. K. Antitumour metal compounds: more than theme and variations. *Dalton Trans.* **2008**, 183−194.

(2) Chu, G. Cellular responses to cisplatin. The roles of DNA-binding proteins and DNA repair. *J. Biol. Chem.* **1994**, *269*, 787−790.

(3) Clarke, M. J. Ruthenium metallopharmaceuticals. *Coord. Chem. Rev.* **2003**, *236*, 209−233.

(4) Alessio, E. Thirty years of the drug candidate NAMI-A and the myths in the field of ruthenium anticancer compounds: A personal perspective. *Eur. J. Inorg. Chem.* **2017**, *2017*, 1549−1560.

(5) Hartinger, C. G.; Jakupec, M. A.; Zorbas-Seifried, S.; Groessl, M.; Egger, A.; Berger, W.; Zorbas, H.; Dyson, P. J.; Keppler, B. K. KP1019, a new redox-active anticancer agent−Preclinical development and results of a clinical phase I study in tumor patients. *Chem. Biodiversity* **2008**, *5*, 2140−2155.

(6) Hartinger, C. G.; Zorbas-Seifried, S.; Jakupec, M. A.; Kynast, B.; Zorbas, H.; Keppler, B. K. From bench to bedside − preclinical and early clinical development of the anticancer agent indazolium trans-[tetrachlorobis(1H-indazole)ruthenate(III)] (KP1019 or FFC14A). *J. Inorg. Biochem.* **2006**, *100*, 891−904.

(7) Rademaker-Lakhai, J. M.; Bongard, D. V. D.; Pluim, D.; Beijnen, J. H.; Schellens, J. H. M. A phase I and pharmacological study with imidazolium-*trans*-DMSO-imidazole-tetrachlororuthenate, a novel ruthenium anticancer agent. *Clin. Cancer Res.* **2004**, *10*, 3717−3727.

(8) Ang, W. H.; Casini, A.; Sava, G.; Dyson, P. J. Organometallic ruthenium-based antitumor compounds with novel modes of action. *J. Organomet. Chem.* **2011**, *696*, 989−998.

(9) Hartinger, C. G.; Dyson, P. J. Bioorganometallic chemistry-from teaching paradigms to medicinal applications. *Chem. Soc. Rev.* **2009**, *38*, 391−401.

(10) Aird, R. E.; Cummings, J.; Ritchie, A. A.; Muir, M.; Morris, R. E.; Chen, H.; Sadler, P. J.; Jodrell, D. I. *In vitro* and *in vivo* activity and cross resistance profiles of novel ruthenium(II) organometallic arene complexes in human ovarian cancer. *Br. J. Cancer* **2002**, *86*, 1652−1657.

(11) (a) Morris, R. E.; Aird, R. E.; del Socorro Murdoch, P.; Chen, H.; Cummings, J.; Hughes, N. D.; Parsons, S.; Parkin, A.; Boyd, G.; Jodrell, D. I.; Sadler, P. J. Inhibition of cancer cell growth by ruthenium(II) arene complexes. *J. Med. Chem.* **2001**, *44*, 3616−3621. (b) Biancalana, L.; Batchelor, L. K.; Funaioli, T.; Zacchini, S.; Bortoluzzi, M.; Pampaloni, G.; Dyson, P. J.; Marchetti, F. α-Diimines as versatile, derivatizable ligands in ruthenium(II)-*p*-cymene anticancer complexes. *Inorg. Chem.* **2018**, *57* (11), 6669−6685.

(12) Schug, K. A.; Lindner, W. Noncovalent binding between guanidinium and anionic groups: Focus on biological- and synthetic-based arginine/guanidinium interactions with phosph[on]ate and sulf[on]ate residues. *Chem. Rev.* **2005**, *105*, 67−113.

(13) Chern, J.; Leu, Y.; Wang, S.; Jou, R.; Hsu, S.; Liaw, Y.; Lin, H. Synthesis and cytotoxic evaluation of substituted sulfonyl-N-hydroxyguanidine derivatives as potential antitumor agents. *J. Med. Chem.* **1997**, *40*, 2276−2286.

(14) Brzozowski, Z.; Saczewski, F.; Gdaniec, M. Synthesis, molecular structure and anticancer activity of 1-allyl-3-amino-2-(4-chloro-2-mercaptobenzenesulphonyl)guanidine derivatives. *Eur. J. Med. Chem.* **2002**, *37*, 285−293.

(15) Dolzhenko, A. V.; Tan, B. J.; Dolzhenko, A. V.; Chiu, G. N. C.; Chui, W. K. Synthesis and biological activity of fluorinated 7-aryl-2-pyridyl6,7-dihydro[1,2,4]triazolo[1,5-a][1,3,5]triazin-5-amines. *J. Fluorine Chem.* **2008**, *129*, 429−434.

(16) Murtaza, G.; Badshah, A.; Said, M.; Khan, H.; Khan, A.; Khan, S.; Siddiq, S.; Choudhary, M. I.; Boudreau, J.; Fontaine, F. G. Urease inhibition and anti-leishmanial assay of substituted benzoylguanidines and their copper(II) complexes. *Dalton Trans.* **2011**, *40*, 9202−9211.

(17) De Vries, N.; Davison, C. E. Technetium nitrido complexes with amine and thiolate ligands: Structural characterization of nitridobis(1,1,2,2-tetramethylguanidine)bis(2,3,5,6-tetramethylbenzenethiolato)technetium, a complex with coordinatively bound 1,1,2,2-tetramethylguanidine. *Inorg. Chem.* **1990**, *29*, 1348−1352.

(18) Fehlhammer, W. P.; Metzner, R.; Sperber, W. Metal complexes of functional isocyanides, XXIV. - Reactions of N-isocyanodialkylamine complexes with secondary amines. *Chem. Ber.* **1994**, *127*, 829−833.

(19) Bailey, P. J.; Mitchell, L. A.; Parsons, S. Guanidine anions as chelating ligands; Syntheses and crystal structures of [Rh(η-C_5Me_5)-{η^2-$(NPh)_2CNHPh$}Cl] and [Ru(η-MeC_6H_4Pri-p)-{η^2-$(NPh)_2CNHPh$}Cl]. *J. Chem. Soc., Dalton Trans.* **1996**, 2839−2841.

(20) Cotton, F. A.; Feng, X.; Timmons, D. J. Further study of very close nonbonded Cu^I−Cu^I contacts. Molecular structure of a new compound and density functional theory calculations. *Inorg. Chem.* **1998**, *37*, 4066−4069.

(21) Dinger, M. B.; Henderson, W. The first mononuclear triazatrimethylenemethane metal complex, [Pt{NPhC(NPh)NPh}-(cod)] (cod = cycloocta-1,5-diene). *Chem. Commun.* **1996**, 211−212.

(22) Bailey, P. J.; Blake, A. J.; Kryszczuk, M.; Parsons, S.; Reed, D. The first triazatrimethylenemethane dianion: Crystal structure of dilithio-triphenylguanidine $Li_2[C(NPh)_3]$ as its tetrahydrofuran solvate. *J. Chem. Soc., Chem. Commun.* **1995**, 1647−1648.

(23) Habtemariam, A.; Melchart, M.; Fernandez, R.; Parsons, S.; Oswald, I. D. H.; Parkin, A.; Fabbiani, F. P. A.; Davidson, J. E.; Dawson, A.; Aird, R. E.; Jodrell, D. I.; Sadler, P. J. Structure−activity relationships for cytotoxic ruthenium(II) arene complexes containing N,N-, N,O-, and O,O-Chelating Ligands. *J. Med. Chem.* **2006**, *49*, 6858−6868.

(24) Jeyalakshmi, K.; Selvakumaran, N.; Bhuvanesh, N. S. P.; Sreekanth, A.; Karvembu, R. DNA/protein binding and cytotoxicity studies of copper(II) complexes containing N, N′, N″-trisubstituted guanidine ligands. *RSC Adv.* **2014**, *4*, 17179−17195.

(25) Jeyalakshmi, K.; Arun, Y.; Bhuvanesh, N. S. P.; Perumal, P. T.; Sreekanth, A.; Karvembu, R. DNA/protein binding, DNA cleavage, cytotoxicity, superoxide radical scavenging and molecular docking studies of copper(II) complexes containing N-benzyl-N′-aryl-N″-benzoylguanidine ligands. *Inorg. Chem. Front.* **2015**, *2*, 780−798.

(26) Murtaza, G.; Rauf, M. K.; Badshah, A.; Ebihara, M.; Said, M.; Gielen, M.; de Vos, D.; Dilshad, E.; Mirza, B. Synthesis, structural characterization and *in vitro* biological screening of some homoleptic copper(II) complexes with substituted guanidines. *Eur. J. Med. Chem.* **2012**, *48*, 26−35.

(27) Sheeba, M. M.; Muthu Tamizh, M.; Farrugia, L. J.; Endo, A.; Karvembu, R. Chiral (η^6-*p*-cymene)ruthenium(II) complexes containing monodentate acylthiourea ligands for efficient asymmetric transfer hydrogenation of ketones. *Organometallics* **2014**, *33*, 540−550.

DOI: 10.1021/acs.organomet.8b00702
Organometallics XXXX, XXX, XXX−XXX

(28) Martinez-Alonso, M. M.; Busto, N.; Jalon, F. A.; Manzano, B. R.; Leal, J. M.; Rodriguez, A. M.; Garcia, B.; Espino, G. Derivation of structure−activity relationships from the anticancer properties of ruthenium(II) arene complexes with 2-aryldiazole ligands. *Inorg. Chem.* **2014**, *53*, 11274−11288.
(29) Kurzwernhart, A.; Kandioller, W.; Bachler, S.; Bartel, C.; Martic, S.; Buczkowska, M.; Muhlgassner, G.; Jakupec, M. A.; Kraatz, H. B.; Bednarski, P. J.; Arion, V. B.; Marko, D.; Keppler, B. K.; Hartinger, C. G. Structure−activity relationships of targeted $Ru^{II}(\eta^6$-*p*-cymene) anticancer complexes with flavonol-derived ligands. *J. Med. Chem.* **2012**, *55*, 10512−10522.
(30) Mohamed Subarkhan, M. K.; Ramesh, R.; Liu, Y. Synthesis and molecular structure of arene ruthenium(II)benzhydrazone complexes: Impact of substitution at chelating ligand and arene moiety on antiproliferative activity. *New J. Chem.* **2016**, *40*, 9813−9823.
(31) Adhireksan, Z.; Davey, G. E.; Campomanes, P.; Groessl, M.; Clavel, C. M.; Yu, H.; Nazarov, A. A.; Yeo, C. H. F.; Ang, W. H.; Droge, P.; Rothlisberger, U.; Dyson, P. J.; Davey, C. A. Ligand substitutions between ruthenium−cymene compounds can control protein *versus* DNA targeting and anticancer activity. *Nat. Commun.* **2014**, *5*, 3462−3475.
(32) Ramakrishnan, S.; Palaniandavar, M. Interaction of rac-$[Cu(diimine)_3]^{2+}$ and rac-$[Zn(diimine)_3]^{2+}$ complexes with CT DNA: Effect of fluxional Cu(II) geometry on DNA binding, ligand−promoted exciton coupling and prominent DNA cleavage. *Dalton Trans.* **2008**, 3866−3878.
(33) Ramachandran, E.; Senthil Raja, D.; Bhuvanesh, N. S. P.; Natarajan, K. Mixed ligand palladium(II) complexes of 6-methoxy-2-oxo-1,2-dihydroquinoline-3-carbaldehyde 4N-substituted thiosemicarbazones with triphenylphosphine co-ligand: Synthesis, crystal structure and biological properties. *Dalton Trans.* **2012**, *41*, 13308−13323.
(34) Senthil Raja, D.; Bhuvanesh, N. S. P.; Natarajan, K. A novel water soluble ligand bridged cobalt(II) coordination polymer of 2-oxo-1,2-dihydroquinoline-3-carbaldehyde (isonicotinic) hydrazone: evaluation of the DNA binding, protein interaction, radical scavenging and anticancer activity. *Dalton Trans.* **2012**, *41*, 4365−4377.
(35) Senthil Raja, D.; Paramaguru, G.; Bhuvanesh, N. S. P.; Reibenspies, J. H.; Renganathan, R.; Natarajan, K. Effect of terminal N-substitution in 2-oxo-1,2-dihydroquinoline-3-carbaldehyde thiosemicarbazones on the mode of coordination, structure, interaction with protein, radical scavenging and cytotoxic activity of copper(II) complexes. *Dalton Trans.* **2011**, *40*, 4548−4559.
(36) Senthil Raja, D.; Bhuvanesh, N. S. P.; Natarajan, K. Biological evaluation of a novel water soluble sulphur bridged binuclear copper(II) thiosemicarbazone complex. *Eur. J. Med. Chem.* **2011**, *46*, 4584−4594.
(37) Eftink, M. R.; Ghiron, C. A. Fluorescence quenching of indole and model micelle systems. *J. Phys. Chem.* **1976**, *80*, 486−493.
(38) Ganeshpandian, M.; Loganathan, R.; Suresh, E.; Riyasdeen, A.; Akbarsha, M. A.; Palaniandavar, M. New ruthenium(II) arene complexes of anthracenylappended diazacycloalkanes: Effect of ligand intercalation and hydrophobicity on DNA and protein binding and cleavage and cytotoxicity. *Dalton Trans.* **2014**, *43*, 1203−1219.
(39) Singh, S. K.; Joshi, S.; Singh, A. R.; Saxena, J. K.; Pandey, D. S. DNA binding and topoisomerase II inhibitory activity of water-soluble ruthenium(II) and rhodium(III) complexes. *Inorg. Chem.* **2007**, *46* (25), 10869−10876.
(40) Haribabu, J.; Sabapathi, G.; Muthu Tamizh, M.; Balachandran, C.; Bhuvanesh, N. S. P.; Venuvanalingam, P.; Karvembu, R. Water-Soluble mono- and binuclear Ru(η^6-*p*-cymene) complexes containing indole thiosemicarbazones: Synthesis, DFT modeling, biomolecular interactions, and *in vitro* anticancer activity through apoptosis. *Organometallics* **2018**, *37*, 1242−1257.
(41) Jeyalakshmi, K.; Haribabu, J.; Bhuvanesh, N. S. P.; Karvembu, R. Half-sandwich $RuCl_2(\eta^6$-*p*-cymene) core complexes containing sulfur donor aroylthiourea ligands: DNA and protein binding, DNA cleavage and cytotoxic studies. *Dalton Trans.* **2016**, *45*, 12518−12531.
(42) Jeyalakshmi, K.; Haribabu, J.; Balachandran, C.; Bhuvanesh, N. S. P.; Emi, N.; Karvembu, R. Synthesis of Ru(II)−benzene complexes containing aroylthiourea ligands, and their binding with biomolecules and *in vitro* cytotoxicity through apoptosis. *New J. Chem.* **2017**, *41* (7), 2672−2686.
(43) Chen, G. Z.; Huang, X. Z.; Xu, J. G.; Wang, Z. B.; Zhang, Z. Z. *Method of Fluorescent Analysis*, 2nd ed; Science Press: Beijing, 1990; p 123, 126 (Chapter 4).
(44) Lucas, S. J.; Lord, R. M.; Wilson, R. L.; Phillips, R. M.; Sridharan, V.; McGowan, P. C. Synthesis of iridium and ruthenium complexes with (N, N), (N, O) and (O, O) coordinating bidentate ligands as potential anti-cancer agents. *Dalton Trans.* **2012**, *41*, 13800−13802.
(45) Khan, R. A.; Arjmand, F.; Tabassum, S.; Monari, M.; Marchetti, F.; Pettinari, C. Organometallic ruthenium(II) scorpionate as topo IIa inhibitor; *In vitro* binding studies with DNA, HPLC analysis and its anticancer activity. *J. Organomet. Chem.* **2014**, *771*, 47−58.
(46) Caruso, F.; Monti, E.; Matthews, J.; Rossi, M.; Gariboldi, M. B.; Pettinari, C.; Pettinari, R.; Marchetti, F. Synthesis, characterization, and antitumor activity of water-soluble (arene)ruthenium(II) derivatives of 1,3-dimethyl-4-acylpyrazolon-5-ato ligands. First example of Ru(arene)(ligand) antitumor species involving simultaneous Ru−N7(guanine) bonding and ligand intercalation to DNA. *Inorg. Chem.* **2014**, *53*, 3668−3677.
(47) Pettinari, R.; Marchetti, F.; Di Nicola, C.; Pettinari, C.; Galindo, A.; Petrelli, R.; Cappellacci, L.; Cuccioloni, M.; Bonfili, L.; Eleuteri, A. M.; Guedes da Silva, M. F. C.; Pombeiro, A. J. L. Ligand design for N, O- or N, N-pyrazolone-based hydrazones ruthenium-(II)-arene complexes and investigation of their anticancer activity. *Inorg. Chem.* **2018**, *57*, 14123−14133.
(48) Nikolic, S.; Opsenica, D. M.; Filipovic, V.; Dojcinovic, B.; Arandelovic, S.; Radulovic, S.; Grguric-Sipka, S. Strong *in vitro* cytotoxic potential of new ruthenium−cymene complexes. *Organometallics* **2015**, *34*, 3464−3473.
(49) Kurzwernhart, A.; Kandioller, W.; Bachler, S.; Bartel, C.; Martic, S.; Buczkowska, M.; Muhlgassner, G.; Jakupec, M. A.; Kraatz, H.-B.; Bednarski, P. J.; Arion, V. B.; Marko, D.; Keppler, B. K.; Hartinger, C. G. Structure−activity relationships of targeted RuII(η^6-*p*-cymene) anticancer complexes with flavonol-derived ligands. *J. Med. Chem.* **2012**, *55*, 10512−10522.
(50) Caruso, F.; Rossi, M.; Benson, A.; Opazo, C.; Freedman, D.; Monti, E.; Gariboldi, M. B.; Shaulky, J.; Marchetti, F.; Pettinari, R.; Pettinari, C. Ruthenium−arene complexes of curcumin: X-Ray and Density Functional Theory structure, synthesis, and spectroscopic characterization, *in vitro* antitumor activity, and DNA docking studies of (*p*-cymene)Ru(curcuminato)chloro. *J. Med. Chem.* **2012**, *55*, 1072−1081.
(51) Meier, S. M.; Hanif, M.; Adhireksan, Z.; Pichler, V.; Novak, M.; Jirkovsky, E.; Jakupec, M. A.; Arion, V. B.; Davey, C. A.; Keppler, B. K.; Hartinger, C. G. Novel metal(II) arene 2-pyridinecarbothioamides: A rationale to orally active organometallic anticancer agents. *Chem. Sci.* **2013**, *4*, 1837−1846.
(52) Kerr, J. F. R.; Wyllie, A. H.; Currie, A. R. Apoptosis: A basic biological phenomenon with wide ranging implications in tissue kinetics. *Br. J. Cancer* **1972**, *26*, 239−257.
(53) Wyllie, A. H. Glucocorticoid-induced thymocyte apoptosis is associated with endogenous endonuclease activation. *Nature* **1980**, *284*, 555−556.
(54) Wyllie, H. A.; Kerr, J. F.; Currie, A. R. Cell death: The significance of apoptosis. *Int. Rev. Cytol.* **1980**, *68*, 251−306.
(55) Cunha, S.; Costa, M. B.; Napolitano, H. B.; Lariucci, C.; Vencato, I. Study of N-benzoyl-activation in the $HgCl_2$-promoted guanylation reaction of thioureas. Synthesis and structural analysis of N-benzoyl-guanidines. *Tetrahedron* **2001**, *57*, 1671−1675.
(56) Petrovic, A.; Milutinovic, M. M.; Petri, E. T.; Zivanovic, M.; Milivojevic, N.; Puchta, R.; Scheurer, A.; Korzekwa, J.; Klisuric, O. R.; Bogojeski, J. Synthesis of camphor-derived bis(pyrazolylpyridine) rhodium(III) complexes: Structure−reactivity relationships and biological activity. *Inorg. Chem.* **2019**, *58*, 307.

DOI: 10.1021/acs.organomet.8b00702
Organometallics XXXX, XXX, XXX−XXX

(57) *APEX2*, Program for Data Collection and Integration on Area Detectors; Bruker AXS Inc.: Madison, WI.
(58) Sheldrick, G. M. *SADABS* (version 2014/5), TWINABS (version 2012/1), Program for Absorption Correction for Data from Area Detector Frames, University of Gottingen, 2014.
(59) Sheldrick, G. M. A short history of SHELX. *Acta Crystallogr., Sect. A: Found. Crystallogr.* **2008**, *A64*, 112−122.
(60) Sheldrick, G. M. SHELXT − Integrated space-group and crystal-structure determination. *Acta Crystallogr., Sect. A: Found. Adv.* **2015**, *A71*, 3−8.
(61) Dolomanov, O. V.; Bourhis, L. J.; Gildea, R. J.; Howard, J. A. K.; Puschmann, H. OLEX2: A complete structure solution, refinement and analysis program. *J. Appl. Crystallogr.* **2009**, *42*, 339−341.
(62) Balachandran, C.; Sangeetha, B.; Duraipandiyan, V.; Raj, M. K.; Ignacimuthu, S.; Al-Dhabi, N. A.; Balakrishna, K.; Parthasarathy, K.; Arulmozhi, N. M.; Arasu, M. V. A flavonoid isolated from Streptomyces sp. (ERINLG-4) induces apoptosis in human lung cancer A549 cells through p53 and cytochrome c release caspase dependent pathway. *Chem.-Biol. Interact.* **2014**, *224*, 24−35.
(63) Akiyama, H.; Endo, M.; Matsui, T.; Katsuda, I.; Emi, N.; Kawamoto, Y.; Koike, T.; Beppu, H. Agaritine from Agaricus blazei Murrill induces apoptosis in the leukemic cell line U937. *Biochim. Biophys. Acta, Gen. Subj.* **2011**, *1810* (5), 519−525.
(64) (a) Balachandran, C.; Emi, N.; Arun, Y.; Yamamoto, Y.; Ahilan, B.; Sangeetha, B.; Duraipandiyan, V.; Inaguma, Y.; Okamoto, A.; Ignacimuthu, S.; Al-Dhabi, N. A.; Perumal, P. T. In vitro anticancer activity of methyl caffeate isolated from Solanum torvum Swartz. Fruit. *Chem.-Biol. Interact.* **2015**, *242*, 81−90. (b) Balachandran, C.; Haribabu, J.; Jeyalakshmi, K.; Bhuvanesh, N. S. P.; Karvembu, R.; Emi, N.; Awale, S. Nickel(II) bis(isatin thiosemicarbazone) complexes induced apoptosis through mitochondrial signaling pathway and G0/G1 cell cycle arrest in IM-9 cells. *J. Inorg. Biochem.* **2018**, *182*, 208−221.

DOI: 10.1021/acs.organomet.8b00702
Organometallics XXXX, XXX, XXX−XXX